Throughput Enhancement in FD- and SWIPT-enabled IoT Networks over Non-Identical Rayleigh Fading Channels

Tan N. Nguyen, *Member, IEEE*, Dinh-Hieu Tran, *Graduate Student Member, IEEE*, Van-Duc Phan*, Miroslav Voznak, *Senior Member, IEEE*, Symeon Chatzinotas, *Senior Member, IEEE*, Björn Ottersten, *Fellow, IEEE*, and H. Vincent Poor, *Life Fellow, IEEE*,
*Corresponding author: Van-Duc Phan (Email: duc.pv@vlu.edu.vn)

***Abstract*—Simultaneous wireless information and power transfer (SWIPT) and full-duplex (FD) communications have emerged as prominent technologies in overcoming the limited energy resources in Internet-of-Things (IoT) networks and improving their spectral efficiency (SE). The article investigates the outage and throughput performance for a decode-and-forward (DF) relay SWIPT system, which consists of one source, multiple relays, and one destination. The relay nodes in this system can harvest energy from the source's signal and operate in FD mode. A sub-optimal, low-complexity, yet efficient relay selection scheme is also proposed. Specifically, a single relay is selected to convey information from a source to a destination so that it achieves the best channel from the source to the relays. An analysis of outage probability (OP) and throughput performed on two relaying strategies, termed static power splitting-based relaying (SPSR) and optimal dynamic power splitting-based relaying (ODPSR), is presented. Notably, we considered independent and non-identically distributed (i.n.i.d.) Rayleigh fading channels, which pose new challenges in obtaining analytical expressions. In this context, we derived exact closed-form expressions of the OP and throughput of both SPSR and ODPSR schemes. We also obtained the optimal power splitting ratio of ODPSR for maximizing the achievable capacity at the destination. Finally, we present extensive numerical and simulation results to confirm our analytical findings. Both simulation and analytical results show the superiority of ODPSR over SPSR.**

***Index Terms*—Full duplex, Internet of Things (IoT), independent and non-identically distributed (i.n.i.d), performance analysis, Rayleigh fading, SWIPT.**

Tan N. Nguyen is at the Communication and Signal Processing Research Group, Faculty of Electrical and Electronics Engineering, Ton Duc Thang University, Ho Chi Minh City, Vietnam. (e-mail: nguyennhattan@tdtu.edu.vn).

Dinh-Hieu Tran, Symeon Chatzinotas, and Björn Ottersten are at the Interdisciplinary Centre for Security, Reliability and Trust (SnT), the University of Luxembourg, Luxembourg, (e-mail: {hieu.tran-dinh, symeon.chatzinotas, bjorn.ottersten } @uni.lu).

Van-Duc Phan is at the Faculty of Automobile Technology, Van Lang University, Ho Chi Minh City, Vietnam, (email: duc.pv@vlu.edu.vn).

Miroslav Voznak is at the VSB Technical University of Ostrava, 17. listopadu 2172/15, 708 00 Ostrava, Czech Republic. (e-mail: miroslav.voznak@vsb.cz).

H. V. Poor is at the Department of Electrical and Computer Engineering at Princeton University, NJ 08544, (email: poor@princeton.edu).

Corresponding author: Van-Duc Phan, (email: duc.pv@vlu.edu.vn).

The research was supported by the Ministry of Education, Youth and Sports of the Czech Republic under the grant SP2021/25 and e-INFRA CZ (ID:90140).

I. Introduction

The Internet of things (IoT) has received substantial attention from academia and industry because it is a promising communications paradigm which can potentially boost the quality of life with advances in smart transportation, manufacturing, smart cities, energy, health care, agriculture, and retail [1]–[3]. Particularly, IoT plays an important key role in fifth generation and beyond, i.e., sixth-generation (6G) systems [4]. Besides many advantages, IoT users usually have limited energy budgets due to their mobility nature and use in remote working environments. Moreover, the explosive increase of resource-intensive IoT applications such as multi-view video construction, augmented reality (AR), virtual reality (VR), and interactive gaming imposes more stringent demands on energy consumption and can significantly reduce the device lifetime. Fortunately, energy harvesting (EH) is a promising solution to overcome the aforementioned problems in IoT networks. In contrast to environmental energy sources such as solar [5] and wind, radio frequency (RF) EH is potential because of its manageability and predictability [6], [7].

RF EH techniques can be divided into wireless power transfer (WPT) [8]–[11] and simultaneous wireless information and power transfer (SWIPT) categories. The main distinction between WPT and SWIPT is that the transmitter's RF signals carry only power in WPT, while it can carry both information and power concurrently in SWIPT. Therefore, SWIPT brings more utilities than WPT but also presents more design challenges since it needs to allocate the harvested energy and information transmission to IoT users. Varshney [12] originated the SWIPT concept and Pulkit Grover and Anant Sahai [13] extended the work to frequency-selective channels with additive white Gaussian noise (AWGN). Nevertheless, [12] and [13] only provided theoretical limits, which was impractical because the electric circuit used to harvest energy from an RF signal could not decode the carried information. To overcome the limitations in [12] and [13], Zhang and Ho [14] proposed two practical receiver designs, termed time switching (TS) and static power splitting (SPS), to schedule the wireless power transfer (WPT) and wireless information transfer (WIT) at the EH receiver.

Recently, extensive studies have been performed to investigate SWIPT with cooperative relaying communications since the SWIPT relay network can improve the communication range and provide power to energy-restricted users. Moreover, the benefits of SWIPT in communication networks have been thoroughly discussed in [15]. The SWIPT relay network can be divided into two types: time switching (TS)-based relaying [16]–[18] and power splitting (PS)-based relaying [19]–[25]. Specifically, Nasir et al. [16] proposed TS-based EH and information transmission (IT) protocols with continuous-time EH and discrete-time EH modes at the relay. They then derived the analytical expressions in terms of throughput for the proposed protocols. Focusing on the TS architecture, the authors in [17] proposed novel relaying protocols based on adaptive TS for amplify-and-forward (AF) and decode-and-forward (DF) modes. In contrast to the studies in [16] and [17], which only considered a simple static TS structure, [18] divided the total time T into N equal time slots and optimized the TS factor in all time slots. Making use of a PS-based EH receiver architecture, a novel system model in which a massive multi-input multi-output (MIMO) two-way relaying system with a PS relay was considered in [19]. By taking into account the Nakagami-m and Rayleigh fading channel, Tan et al. [20] analyzed the performance analysis of user selection protocols with PS-based EH. Differently from [19] and [20], which only considered a static PS factor, [21] and [22] designed relay selection schemes based on an optimal dynamic PS ratio. While [19]–[22] only considered TS- or PS-based relaying schemes, [23] and [24] investigated a two-way half-duplex hybrid time-switching and power-splitting (HTPSR) relay network which leveraged the advantages of both TS and PS protocols. Besides, Liu et al [25] aimed to maximize the 5G and IoT transmission rate and the total power consumption by jointly optimizing time/power allocation factors and transmit powers. In [26], the authors proposed a practical non-linear EH model in SWIPT systems, where they aimed to maximize the total harvested energy at the EH receivers according to the minimum demanded signal-to-interference-plus-noise ratios at the information receivers.

The above works on SWIPT relay networks are discussed in the context of half-duplex (HD) scenarios in which half of the time or frequency resources are wasted [27]. However, advances in self-interference cancellation (SIC) techniques achieve more than 110 dB reduction of self-interference [28]–[31]. Therefore, full-duplex (FD) communication may be considered a potential spectral efficiency (SE) enhancement technique for future 5G/6G systems [32], [33]. The combination of SWIPT techniques and FD for cooperative relaying systems was studied in [34]–[39]. Tan et al. [34] investigated a DF FD adaptive relaying network over a Rician fading environment with SWIPT. Specifically, in the first time slot, the relay harvested energy from the source node. In the second time slot, a portion of power was used for EH in combination with the PS method, and the other portion was scheduled for relaying data from the source to destination. The integration of physical layer security together with FD and SWIPT was studied in [35], [36]. In [35], the secrecy sum rate maximization problem for OFDMA with PS-SWIPT and TDMA with TS-SWIPT under perfect and imperfect CSI was investigated. In [36], sum-information-transmission-rate-maximization (SITRM) and fairness-aware-SITRM problems were studied, whereas multiple eavesdroppers could overhear information from the FD base station and FD users. An accumulated loopback self-interference (ALSI) under the AF protocol in a two-way FD relaying system with SWIPT was first proposed and investigated in [37]. In [38], self-energy recycling was applied to improve the network performance of an FD wireless-powered AF relaying system.

Note that for simplicity, all the aforementioned works on FD SWIPT relay systems [34]–[39] only consider traditional independent and identically distributed (i.i.d.) fading channels. Moreover, few works apply an independent and non-identically distributed (i.n.i.d.) fading model because of the difficulty in obtaining the closed-form expressions. Motivated by these observations, our work presents a generalized FD SWIPT relay network which models the transmission channels with i.n.i.d. Rayleigh fading. The main contributions of this work can be summarized as follows:

- We propose and thoroughly study the benefits of two cooperative relaying schemes: (i) static power splitting-based relaying (SPSR); (ii) optimal dynamic power splitting-based relaying (ODPSR).
- To the best of our knowledge, this is the first work which obtains closed-form expressions for the outage probability (OP) and system throughput in DF-based FD SWIPT cooperative networks over non-identical fading channels. This is particularly challenging since the mathematical analysis involves many random variables and the model channel uses i.n.i.d. Rayleigh fading, thereby complicating derivation.
- We present a mathematical analysis for the optimal value of the power splitting ratio $\rho^\star$ to maximize the destination's capacity, i.e., $\mathrm{C_{DF}}$. Specifically, since we consider the DF protocol, the $\rho^\star$ can be obtained by equalizing the signal-to-noise ratio (SNR) on the first and second hop. Notably, $\rho^\star$ is achieved before data transmission begins.
- Our analytical expressions are corroborated through Monte Carlo simulations. The simulation results show the superiority of ODPSR compared to SPSR.

The remainder of the paper is organized as follows. The system model and problem formulation are given in Section II. The derivation of key performance metrics, including the OP and throughput of the proposed model, is presented in Section III. Numerical results are shown in Section IV. Section V concludes the paper.

II. System Model

In this model, a source S communicates with the destination D with the assistance of full-duplex relays denoted by R_m, where $m = \{1, \ldots, M\}$.

This article has been accepted for publication in a future issue of this journal, but has not been fully edited. Content may change prior to final publication. Citation information: DOI 10.1109/JIOT.2021.3120766, IEEE Internet of Things Journal

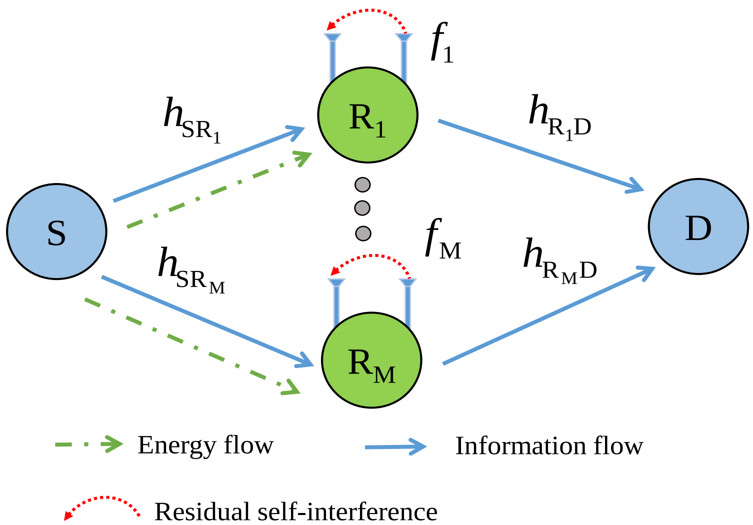

Fig. 1: System model

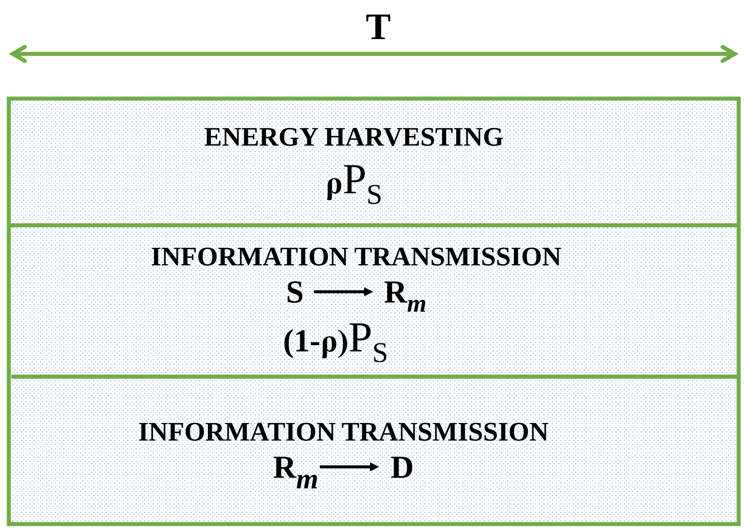

Fig. 2: Schematic illustration of EH and IT processes with a power splitting relaying protocol at the relay

Let us denote h_{SR_m} and $h_{\mathrm{R}_m\mathrm{D}}$ as the channel coefficients between $\mathrm{S} \rightarrow \mathrm{R}_m$ and $\mathrm{R}_m \rightarrow \mathrm{D}$ links, respectively. We also denote the self-interference between the transmit antenna and the receive antenna of the relay R_m.

Let us assume that all the channels are independent and non-identical (i.n.i.d.) Rayleigh fading, hence the channel gains $\gamma_{\mathrm{SR}_m} = |h_{\mathrm{SR}_m}|^2$ and $\gamma_{\mathrm{R}_m\mathrm{D}} = |h_{\mathrm{R}_m\mathrm{D}}|^2$ are exponential random variables (RVs) whose CDF are given as

$$F_{\gamma_{\mathrm{SR}_m}}(x) = 1 - \exp\left(-\lambda_{\mathrm{SR}_m} x\right), \quad (1)$$

$$F_{\gamma_{\mathrm{R}_m\mathrm{D}}}(x) = 1 - \exp\left(-\lambda_{\mathrm{R}_m\mathrm{D}} x\right). \quad (2)$$

The physical meaning of the parameters $\lambda_{\mathrm{S}_m\mathrm{R}}$ or $\lambda_{\mathrm{R}_m\mathrm{D}}$ is the inverse of the channel power gains. Furthermore, the channel power gain is inversely proportional to the distance between transmitter and receiver, increasing exponentially with the path-loss exponent. In this paper, we apply the simplified path-loss model [40], thus, the parameters $\lambda_{\mathrm{S}_m\mathrm{R}}$ and $\lambda_{\mathrm{R}_m\mathrm{D}}$ can be modeled respectively as follows:

$$\lambda_{\mathrm{SR}_m} = \left(d_{\mathrm{SR}_m}\right)^{\beta}, \quad (3)$$

$$\lambda_{\mathrm{R}_m\mathrm{D}} = \left(d_{\mathrm{R}_m\mathrm{D}}\right)^{\beta}, \quad (4)$$

where d_{SR_m} and $d_{\mathrm{R}_m\mathrm{D}}$ are Euclidean distances between $\mathrm{S} \rightarrow \mathrm{R}_m$ and $\mathrm{R}_m \rightarrow \mathrm{D}$, respectively.

Let us denote f_m as the residual self-interference suppression (SiS) level after interference cancellations, which is modeled as a complex Gaussian RV and $\varphi_m = |f_m|^2$ follows exponential distribution. Therefore, its cumulative distribution function (CDF) can be expressed as

$$F_{\varphi_m}(x) = 1 - \exp\left(-\Omega_m x\right). \quad (5)$$

From (1), (2), and (5), the probability density functions

This article has been accepted for publication in a future issue of this journal, but has not been fully edited. Content may change prior to final publication. Citation information: DOI 10.1109/JIOT.2021.3120766, IEEE Internet of Things Journal

TABLE I: Key Parameters of the System Model

Notations	Descriptions
P_{S}	The average transmit power at the source
P_{R_m}	The average transmit power at the relay R_m
n_{R_m}	The additive white Gaussian noise (AWGN) at the relay R_m
n_{D}	The AWGN at the destination D
Γ_{SR_m}	The SNR at the relay R_m
$\Gamma_{\mathrm{R}_m\mathrm{D}}$	The SNR at the destination D
C_{DF}	The capacity of system
ψ_{DF}	The overall SNR of system
τ	The average achievable throughput at the destination D
OP	The outage probability
T	The time duration
$\gamma_{\mathrm{SR}_m} = \lvert h_{\mathrm{SR}_m}\rvert^2$	The channel gain of $\mathrm{S} \to \mathrm{R}_m$ link
$\gamma_{\mathrm{R}_m\mathrm{D}} = \lvert h_{\mathrm{R}_m\mathrm{D}}\rvert^2$	The channel gain of $\mathrm{R}_m \to \mathrm{D}$ link
$\varphi_m = \lvert f_m\rvert^2$	The channel gain of residual self-interference at the relay R_m
C_{th}	The target rate
γ_{th}	The SNR threshold of the system

(PDFs) of γ_{SR_m}, $\gamma_{\mathrm{R}_m\mathrm{D}}$, and φ_m are respectively given as

$$f_{\gamma_{\mathrm{SR}_m}}(x) = \lambda_{\mathrm{SR}_m} \exp\left(-\lambda_{\mathrm{SR}_m} x\right), \tag{6}$$

$$f_{\gamma_{\mathrm{R}_m\mathrm{D}}}(x) = \lambda_{\mathrm{R}_m\mathrm{D}} \exp\left(-\lambda_{\mathrm{R}_m\mathrm{D}} x\right), \tag{7}$$

$$f_{\varphi_m}(x) = \Omega_m \exp\left(-\Omega_m x\right). \tag{8}$$

Then, the received signal at the m-th relay can be expressed as

$$y_{\mathrm{R}_m} = \sqrt{1-\rho}\, h_{\mathrm{SR}_m} x_{\mathrm{S}} + f_m x_{\mathrm{R}_m} + n_{\mathrm{R}_m}, \tag{9}$$

where $m \in (1, 2, ..., M)$; x_{S} denotes the transmitted signal at the source S such that $\mathbb{E}\{|x_{\mathrm{S}}|^2\} = P_{\mathrm{S}}$, where P_{S} is the average transmit power at the source and $\mathbb{E}\{\bullet\}$ is the expectation operator; $n_{\mathrm{R}_m} \sim \mathcal{CN}(0, N_0)$ is the additive white Gaussian noise (AWGN) at relay R_m; x_{R_m} is the loopback interference signal at R_m due to full-duplex relaying and satisfies $\mathbb{E}\{|x_{\mathrm{R}_m}|^2\} = P_{\mathrm{R}_m}$.

Use of the power splitting method means the transmit power at relay R_m can be mathematically modeled as

$$P_{\mathrm{R}_m} = \frac{\mathrm{E}_m}{\mathrm{T}} = \eta\rho P_{\mathrm{S}} \gamma_{\mathrm{SR}_m}, \tag{10}$$

where $0 < \eta \leq 1$ is the energy conversion coefficient at the relay. The received signal at the destination D can then be given as

$$y_{\mathrm{D}} = h_{\mathrm{R}_m\mathrm{D}} x_{\mathrm{R}_m} + n_{\mathrm{D}}, \tag{11}$$

where n_{D} is the zero mean AWGN with variance N_0 at the destination D.

From (9), the signal to noise ratio (SNR) at the m-th relay can be derived according to

$$\Gamma_{\mathrm{SR}_m} = \frac{(1-\rho)\gamma_{\mathrm{SR}_m} P_{\mathrm{S}}}{\varphi_m P_{\mathrm{R}_m} + N_0}. \tag{12}$$

By substituting (10) into (12), Γ_{SR_m} is re-written as

$$\Gamma_{\mathrm{SR}_m} = \frac{(1-\rho)\gamma_{\mathrm{SR}_m} P_{\mathrm{S}}}{\eta\rho P_{\mathrm{S}} \varphi_m \gamma_{\mathrm{SR}_m} + N_0} \approx \frac{(1-\rho)}{\eta\rho\varphi_m}. \tag{13}$$

Based on (11), the SNR at the destination can be obtained as

$$\Gamma_{\mathrm{R}_m\mathrm{D}} = \frac{P_{\mathrm{SR}_m} \gamma_{\mathrm{R}_m\mathrm{D}}}{N_0} = \eta\rho\Psi\gamma_{\mathrm{SR}_m}\gamma_{\mathrm{R}_m\mathrm{D}}, \tag{14}$$

where

$$\Psi \triangleq \frac{P_s}{N_0}. \tag{15}$$

In the proposed system, we consider the decode-and-forward (DF) technique. Therefore, the overall SNR and the capacity of the system can be respectively given by

$$\psi_{\mathrm{DF}} = \min\left(\Gamma_{\mathrm{SR}_m}, \Gamma_{\mathrm{R}_m\mathrm{D}}\right), \tag{16}$$

$$C_{\mathrm{DF}} = \log_2\left(1 + \psi_{\mathrm{DF}}\right). \tag{17}$$

The average achievable throughput at the destination D can be defined as

$$\tau = (1 - \mathrm{OP}) \times C_{\mathrm{DF}}, \tag{18}$$

where

$$\mathrm{OP} = \Pr\left(\psi_{\mathrm{DF}} < \gamma_{th}\right), \tag{19}$$

$$\gamma_{th} \triangleq 2^{C_{\mathrm{th}}} - 1, \tag{20}$$

are defined as the outage probability and the SNR threshold of the system, respectively. C_{th} is the target rate at the destination to successfully decode the received signals.

Remark 1: In the present paper, we apply the partial relay selection (PRS) method. Specifically, we propose an optimal relay selection protocol in which the best relay user is selected, as follows:

$$\mathrm{R}_a : \gamma_{\mathrm{SR}_a} = \max_{m=1,2,\ldots,M}\left(\gamma_{\mathrm{SR}_m}\right). \tag{21}$$

Because the best relay fails to decode a message from the source is equivalent to the failure of all of the relays, and each relay is independent of the others. Therefore, the CDF of γ_{SR_a} can be expressed as follows [41]:

$$F_{\gamma_{\mathrm{SR}_a}}(x) = \Pr\left(\gamma_{\mathrm{SR}_a} < x\right) = \prod_{m=1}^{M} F_{\gamma_{\mathrm{SR}_m}}(x). \tag{22}$$

Particularly, we consider a generalized system model with i.n.i.d. Rayleigh fading channel such that $\lambda_{\mathrm{SR}_m} \neq \lambda_{\mathrm{SR}_n}, \forall m \neq$

n. Thus, $F_{\gamma_{\mathrm{SR}_a}}(x)$ can be expressed as follows [41]:

$$\begin{aligned} F_{\gamma_{\mathrm{SR}_a}}(x) &= \prod_{m=1}^{M} \left[1-\exp\left(-\lambda_{\mathrm{SR}_m} x\right)\right] \\ &= 1+\sum_{n=1}^{M}(-1)^n \sum_{\substack{\mathrm{SR}_1=\cdots=\mathrm{SR}_n=1,\\ \mathrm{SR}_1<\cdots<\mathrm{SR}_n}}^{M} \exp\left(-\sum_{t=1}^{n}\lambda_{\mathrm{SR}_t} x\right). \end{aligned} \quad (23)$$

III. Outage Probability Analysis

In this section, the outage probability of the FD- and SWIPT-assisted DF relaying system with i.n.i.d. Rayleigh fading channels and PS method is derived. It is noted that the derived mathematical framework can be straightforwardly apply to the TS protocol by modifying some constant numbers, i.e., the target rate and the constant number associates with Γ_{SR_m}.

A. Static Power Splitting-based Relaying (SPSR)

In this case, the power splitting ratio ρ is fixed at a constant value.

By combining (16) and (19), the OP of the SPS-based relaying method can be formulated as in (24) shown at the top of the next page.

Lemma 1: Based on (23), the CDF function of Z_a can be computed as

$$\begin{aligned} F_{Z_a}(x) &= \Pr\left(Z_a<x\right) = \prod_{m=1, m\neq a}^{M}\left(1-\exp\left(-\lambda_{\mathrm{SR}_m}x\right)\right) \\ &= 1+\sum_{u=1}^{M-1}(-1)^u \sum_{\substack{i_1=\cdots=i_u=1,\\ i_1<\cdots<i_u,\\ i_1,\ldots,i_u\neq a}}^{M} \exp\left(-\sum_{v=1}^{u}\lambda_{\mathrm{SR}_{i_v}}x\right) \\ &= 1+\sum_{u=1}^{M-1}(-1)^u \sum_{\substack{i_1=\cdots=i_u=1,\\ i_1<\ldots<i_u,\\ i_1,\ldots,i_u\neq a}}^{M} \exp\left(-\lambda_{a,u}^{\mathrm{sum}}x\right) \end{aligned} \quad (26)$$

where

$$\lambda_{a,u}^{\mathrm{sum}} = \sum_{v=1}^{u}\lambda_{\mathrm{SR}_{i_v}} \quad (27)$$

Lemma 2: Based on (26), the PDF function of Z_a can be computed as

$$f_{Z_a}(x) = \sum_{u=1}^{M-1}(-1)^{u+1} \sum_{\substack{i_1=\ldots=i_u=1,\\ i_1<\ldots<i_u,\\ i_1,\ldots,i_u\neq a}}^{M} \lambda_{a,u}^{\mathrm{sum}}\exp\left(-\lambda_{a,u}^{\mathrm{sum}}x\right). \quad (28)$$

Theorem 1: In the FD SWIPT system which uses the static power splitting method, the exact closed-form expression of OP can be mathematically formulated as in (29), which is shown at the top of next page.

Proof: See Appendix A. ■

B. Optimal Dynamic Power Splitting-based Relaying (ODPSR)

From (16)(18), in order to improve the achievable throughput of system, we find the optimal value of the power splitting ratio $\rho^\star$ to maximize C_{DF}. Since the DF protocol is considered in our work, the optimal power splitting ratio $\rho^\star$ can be obtained as follows:

$$\Gamma_{\mathrm{SR}_m} = \Gamma_{\mathrm{R}_m\mathrm{D}} \leftrightarrow \frac{(1-\rho)}{\eta\rho\varphi_m} = \eta\rho\Psi\gamma_{\mathrm{SR}_m}\gamma_{\mathrm{R}_m\mathrm{D}}. \quad (31)$$

Proof: See Appendix B. ■

Lemma 3: In an FD SWIPT system which uses ODPSR with one source, multiple FD relay nodes, and one destination, the closed-form of optimal power splitting ratio $\rho^\star$ can be given as

$$\rho^\star = \frac{\sqrt{4\eta^2\Psi\varphi_m\gamma_{\mathrm{SR}_m}\gamma_{\mathrm{R}_m\mathrm{D}}+1}-1}{2\eta^2\Psi\varphi_m\gamma_{\mathrm{SR}_m}\gamma_{\mathrm{R}_m\mathrm{D}}}. \quad (32)$$

Proof: See Appendix C. ■

By substituting (32) into (14), we then have

$$\Gamma_{\mathrm{R}_m\mathrm{D}}^\star = \frac{\sqrt{4\eta^2\Psi\varphi_m\gamma_{\mathrm{SR}_m}\gamma_{\mathrm{R}_m\mathrm{D}}+1}-1}{2\eta\varphi_m}. \quad (33)$$

Then, the OP of ODPSR method can be mathematically formulated as

$$\begin{aligned} &\mathrm{OP}_{\mathrm{ODPSR}} \\ &= \sum_{a=1}^{M}\Pr\left(\gamma_{\mathrm{SR}_a} = \max_{m=1,\ldots,M}\left(\gamma_{\mathrm{SR}_m}\right), \Gamma_{\mathrm{R}_m\mathrm{D}}^\star < \gamma_{th}\right) \\ &= \sum_{a=1}^{M}\Pr\left(\begin{array}{r} \gamma_{\mathrm{SR}_a} > Z_a, \\ \dfrac{\sqrt{4\eta^2\Psi\varphi_a\gamma_{\mathrm{SR}_a}\gamma_{\mathrm{R}_a\mathrm{D}}+1}-1}{2\eta\varphi_a} < \gamma_{th} \end{array}\right) \\ &= \sum_{a=1}^{M}\Pr\left(\begin{array}{r} \gamma_{\mathrm{SR}_a} > Z_a, \\ 4\eta^2\Psi\varphi_a\gamma_{\mathrm{SR}_a}\gamma_{\mathrm{R}_a\mathrm{D}}+1 < \left(2\eta\gamma_{th}\varphi_a+1\right)^2 \end{array}\right) \\ &= \sum_{a=1}^{M}\Pr\left(\gamma_{\mathrm{SR}_a} > Z_a, \eta\Psi\gamma_{\mathrm{SR}_a}\gamma_{\mathrm{R}_a\mathrm{D}} < \gamma_{th}(\eta\gamma_{th}\varphi_a+1)\right) \\ &= \sum_{a=1}^{M}\underbrace{\Pr\left(\gamma_{\mathrm{SR}_a} > Z_a, \gamma_{\mathrm{SR}_a}\gamma_{\mathrm{R}_a\mathrm{D}} < \frac{\gamma_{th}(\eta\gamma_{th}\varphi_a+1)}{\eta\Psi}\right)}_{\Upsilon} \end{aligned} \quad (34)$$

From (34), we need to find Υ to obtain the closed-form of $\mathrm{OP}_{\mathrm{ODPSR}}$, which can be given by

$$\Upsilon = \int_{0}^{+\infty}\Omega_a\exp\left(-\Omega_a x\right)\Theta dx, \quad (35)$$

where

$$\Theta \triangleq \Pr\left(\gamma_{\mathrm{SR}_a} > Z_a, \gamma_{\mathrm{SR}_a}\gamma_{\mathrm{R}_a\mathrm{D}} < \frac{\gamma_{th}(\eta\gamma_{th}x+1)}{\eta\Psi}\right). \quad (36)$$

Lemma 4: The closed-form expression of Θ can be given as

$$\Theta = \sum_{u=1}^{M-1}(-1)^{u+1}\sum_{\substack{i_1=\cdots=i_u=1,\\ i_1<\cdots<i_u,\\ i_1,\ldots,i_u\neq a}}^{M}\lambda_1$$

This article has been accepted for publication in a future issue of this journal, but has not been fully edited. Content may change prior to final publication. Citation information: DOI 10.1109/JIOT.2021.3120766, IEEE Internet of Things Journal

$$
\begin{aligned}
\mathrm{OP}_{\mathrm{SPSR}} &= \sum_{a=1}^{M} \Pr\left(\gamma_{\mathrm{SR}_a} = \max_{m=1,2,\dots,M}\left(\gamma_{\mathrm{SR}_m}\right), \psi_{\mathrm{DF}} < \gamma_{\mathrm{th}}\right) \\
&= \sum_{a=1}^{M} \Pr\left(\gamma_{\mathrm{SR}_a} > Z_a, \min\left(\frac{(1-\rho)}{\eta\rho\varphi_a}, \eta\rho\Psi\gamma_{\mathrm{SR}_a}\gamma_{\mathrm{R}_a\mathrm{D}}\right) < \gamma_{\mathrm{th}}\right) \\
&= 1 - \underbrace{\sum_{a=1}^{M} \Pr\left(\gamma_{\mathrm{SR}_a} > Z_a, \frac{(1-\rho)}{\eta\rho\varphi_a} \geq \gamma_{\mathrm{th}}, \eta\rho\Psi\gamma_{\mathrm{SR}_a}\gamma_{\mathrm{R}_a\mathrm{D}} \geq \gamma_{\mathrm{th}}\right)}_{\widetilde{\mathrm{OP}}}, \qquad (24)
\end{aligned}
$$

$$
\text{where } \mathrm{Z_a} = \max_{m=1,2,\dots,M, m\neq a}\left(\gamma_{\mathrm{SR}_m}\right). \qquad (25)
$$

$$
\mathrm{OP}_{\mathrm{SPSR}} = 1 + \sum_{a=1}^{M}\left\{1 - \exp\left[-\frac{\Omega_a(1-\rho)}{\eta\rho\gamma_{\mathrm{th}}}\right]\right\} \times \left\{\sum_{u=1}^{M-1}(-1)^{u+1}\sum_{\substack{i_1=\cdots=i_u=1,\\ i_1<\cdots<i_u,\\ i_1,\dots,i_u\neq a}}^{M}\left[\begin{array}{r}\frac{2\lambda_{\mathrm{SR}_a}}{\lambda_{a,u}^{\mathrm{sum}}+\lambda_{\mathrm{SR}_a}} \times \sqrt{(\lambda_{a,u}^{\mathrm{sum}}+\lambda_{\mathrm{SR}_a})\chi} \\ \times K_1\left(2\sqrt{(\lambda_{a,u}^{\mathrm{sum}}+\lambda_{\mathrm{SR}_a})\chi}\right) \\ -2\sqrt{\lambda_{\mathrm{SR}_a}\chi} \times K_1\left(2\sqrt{\lambda_{\mathrm{SR}_a}\chi}\right)\end{array}\right]\right\}, \qquad (29)
$$

$$
\text{where } \chi \triangleq \frac{\lambda_{\mathrm{R_aD}}\gamma_{\mathrm{th}}}{\eta\rho\Psi}. \qquad (30)
$$

$K_v\{\bullet\}$ is the modified Bessel function of the second kind and v^{th} order.

$$
+\sum_{u=1}^{M-1}(-1)^{u+1}\sum_{\substack{i_1=\cdots=i_u=1,\\ i_1<\cdots<i_u,\\ i_1,\dots,i_u\neq a}}^{M}\Theta_1, \qquad (37)
$$

where

$$
\begin{aligned}
\Theta_1 = {} & \frac{2\lambda_{\mathrm{SR}_a}}{\lambda_{a,u}^{\mathrm{sum}}+\lambda_{\mathrm{SR}_a}}\sqrt{\frac{\left(\lambda_{a,u}^{\mathrm{sum}}+\lambda_{\mathrm{SR}_a}\right)\lambda_{\mathrm{R}_a\mathrm{D}}\gamma_{\mathrm{th}}\left(\eta\gamma_{th}x+1\right)}{\eta\Psi}} \\
& \times K_1\left(2\sqrt{\frac{\left(\lambda_{a,u}^{\mathrm{sum}}+\lambda_{\mathrm{SR}_a}\right)\lambda_{\mathrm{R}_a\mathrm{D}}\gamma_{\mathrm{th}}\left(\eta\gamma_{th}x+1\right)}{\eta\Psi}}\right) \\
& - 2\sqrt{\frac{\lambda_{\mathrm{SR}_a}\gamma_{\mathrm{th}}\lambda_{\mathrm{R}_a\mathrm{D}}\left(\eta\gamma_{th}x+1\right)}{\eta\Psi}} \\
& \times K_1\left(2\sqrt{\frac{\lambda_{\mathrm{SR}_a}\lambda_{\mathrm{R}_a\mathrm{D}}\gamma_{\mathrm{th}}\left(\eta\gamma_{th}x+1\right)}{\eta\Psi}}\right). \qquad (38)
\end{aligned}
$$

Proof: See Appendix D. ■

Lemma 5: Based on Θ from (37), the exact closed-form expression of Υ can be given as

$$
\begin{aligned}
\Upsilon = {} & \sum_{u=1}^{M-1}(-1)^{u+1}\sum_{\substack{i_1=\cdots=i_u=1,\\ i_1<\cdots<i_u,\\ i_1,\dots,i_u\neq a}}^{M}\lambda_1 \\
& + \sum_{t=0}^{\infty}\sum_{u=1}^{M-1}\sum_{\substack{i_1=\cdots=i_u=1,\\ i_1<\cdots<i_u,\\ i_1,\dots,i_u\neq a}}^{M}\frac{(-1)^{t+u+1}\left(\frac{\Omega_a}{\eta\gamma_{th}}\right)^{t+1}\exp\left(\frac{\Omega_a}{\eta\gamma_{th}}\right)}{t!} \\
& \times\left[\begin{array}{c}\frac{\lambda_{\mathrm{SR}_a}\times G_{1,3}^{3,0}\left(\vartheta^2\middle|\begin{array}{c}0\\-1,t+1,t\end{array}\right)}{\left(\lambda_{a,u}^{\mathrm{sum}}+\lambda_{\mathrm{SR}_a}\right)\vartheta^{2t}} \\ -\frac{G_{1,3}^{3,0}\left(\zeta^2\middle|\begin{array}{c}0\\-1,t+1,t\end{array}\right)}{\zeta^{2t}}\end{array}\right], \qquad (39)
\end{aligned}
$$

where $\mathrm{G}_{p,q}^{m,n}\left(z\middle|\begin{array}{c}a_1,\dots,a_p\\b_1,\dots,b_q\end{array}\right)$ is the Meijer G-function.

Proof: See Appendix E. ■

Based on the result obtained in Lemma 5, the OP of DPS can be given as the theorem below.

Theorem 2: In an FD SWIPT system which uses the dynamic power splitting method, the exact closed-form expression of OP can be mathematically formulated as follows:

$$
\mathrm{OP}_{\mathrm{ODPSR}} = \sum_{a=1}^{M}\sum_{u=1}^{M-1}(-1)^{u+1}\sum_{\substack{i_1=\cdots=i_u=1,\\ i_1<\cdots<i_u,\\ i_1,\dots,i_u\neq a}}^{M}\lambda_1 + \sum_{t=0}^{\infty}
$$

TABLE II: Simulation parameters.

Symbol	Parameter name	Value
C_{th}	SNR threshold of the system	1.25
η	Energy harvesting efficiency	0.8
ρ	Power splitting ratio	0.05 to 0.95
λ_{RR}	Rate parameter of $\lvert h_{\mathrm{RR}}\rvert^2$	0.5 to 5
Ψ	Transmit power-to-noise-ratio	-15 to 15 (dB)
M	Number of relays	1 to 4

$$\left[\begin{array}{l} \sum_{a=1}^{M}\sum_{u=1}^{M-1}\sum_{\substack{i_1=\cdots=i_u=1,\\ i_1<\cdots<i_u,\\ i_1,\ldots,i_u\neq a}}^{M} \frac{(-1)^{t+u+1}\times\left(\frac{\Omega_a}{\eta\gamma_{th}}\right)^{t+1}\times\exp\left(\frac{\Omega_a}{\eta\gamma_{th}}\right)}{t!} \\ \times\left(\frac{\lambda_{\mathrm{SR}_a}\times G_{1,3}^{3,0}\left(\vartheta^2\,\middle|\,\begin{matrix}0\\ -1,t+1,t\end{matrix}\right)}{\left(\lambda_{a,u}^{\mathrm{sum}}+\lambda_{\mathrm{SR}_a}\right)\vartheta^{2t}} - \frac{G_{1,3}^{3,0}\left(\zeta^2\,\middle|\,\begin{matrix}0\\ -1,t+1,t\end{matrix}\right)}{\zeta^{2t}}\right) \end{array}\right]. \tag{40}$$

Remark 2: By substituting (29) and (40) into (18), we can obtain the average achievable throughput at the destination for both the static and the dynamic power splitting methods.

IV. Numerical Results

This section presents the numerical results, validation of the analytical expressions with simulations, and a description of the effect on system performance by the various parameters. Unless otherwise stated, we assume the following parameters: threshold rate $\mathrm{C_{th}}$ = 1.25 bps/Hz, static power splitting ratio ρ = 0.3, energy conversion coefficient η = 0.8, Ψ = 5 dB, Ω_a = 0.5, number of relays M = 2, path loss exponent β = 3 [42], [43]. We also assume a unit distance between the source S and destination D. The results were obtained from Monte Carlo simulations with MATLAB [44]. All simulation results were averaged over 10^6 channel realizations. For clarity, the simulation parameter settings are listed in Table II.

Fig. 3 charts the outage probability and throughput versus Ψ of the SPSR and ODPSR schemes for a varying number of relay nodes, where $\mathrm{C_{th}}$ = 1.25 bps/Hz, η = 0.8 and Ω_a = 5. The distance from source S to relay R_m was d_{SR_m} = 0.3 or d_{SR_m} = [0.3, 0.65, 0.8], corresponding to the respective number of relays used. We can observe from Fig. 3 that the outage probability of the SPSR and ODPSR schemes significantly improved as Ψ increased from -15 to 15 dB. Specifically, at Ψ = -15 dB and Ψ = 15 dB for M = 3, the OP of the ODPSR scheme was 0.5333 and 0.0013, respectively, while the SPSR only achieved 0.7866 and 0.0036. This was expected since Ψ is defined as the ratio of the transmit power at the source divided by the noise power. Therefore, the higher Ψ values imply that a higher source transmit power P_s is used. Consequently, a higher SNR at the destination can be obtained, calculated from Eqs. (10) and (14).In addition, by increasing the number of relays from one to three, the outage performance improved dramatically. For example, at Ψ = -15 dB for M = 1 and M = 3, the OP of ODPSR scheme was 0.6024 and 0.533, respectively. This is obvious because we have more opportunities to select the better channel, which improves the network performance.

Fig. 4 plots the total collected throughput versus Ψ of the SPSR and ODPSR schemes for a varying number of relay nodes, where $\mathrm{C_{th}}$ = 1.25 bps/Hz, η = 0.8 and Ω_a = 5. We observe that as the Ψ value increased from -15 to 6 dB, the achievable throughput at the destination improved significantly. Specifically, at Ψ = -15 and -9 dB, the throughput of ODPSR with three relays was 0.5837 and 0.9860 bps/Hz, respectively. This is because the outage value reduced dramatically as Ψ changed from -15 to 6 dB, leading to an improvement in the achievable throughput given by Eq. (18). We can also observe that the throughput of the ODPSR scheme is much higher than the throughput of SPSR. This is because the outage performance of ODPSR is much lower than the OP of SPSR, shown in Fig. 3. Specifically, for M = 3 and Ψ = -15 dB, the throughput of the ODPSR scheme achieved 0.5837 bps/Hz while SPSR obtained less than 54 % throughput, i.e., 0.2667 bps/Hz. Nevertheless, when the value of Ψ is large enough (i.e., $\Psi \geq 15$ dB), the throughput of all algorithms converges to the saturation value. For wireless communication systems, we expect high throughput but low outage probability. Thus, it is necessary to select a suitable value of Ψ to achieve this target. A large value of Ψ may not always benefit since the system cannot be supported because of the limited energy budget, especially in IoT networks. Moreover, it also increases the risk of eavesdropping on important information.

Figs. 5 and 6 chart the OP and throughput versus Ψ for different distances of the relay node to source S, where M = 2, $\mathrm{C_{th}}$ = 1.25 (bps/Hz), η = 0.8, and Ω_a = 5. We observe from Fig. 5 results similar to those in Fig. 3. Specifically, the outage probability of ODPSR still outperforms SPSR methods. SPSR where ρ = 0.3 has better results than SPSR where ρ = 0.7. We can also observe that the closer the distance between the relay nodes and the source node, the better the achieved outage performance. This is because we apply two-hop decode-and-forward relaying, and the overall SNR of the system can be calculated as the minimum of the SNR at relay R_m and the SNR at destination D, as in (16). When the relay nodes are allocated near source S, we thus have more chance of successfully decoding the signal on the first hop, which enhances the OP. If the relay node fails to decrypt the received signals, an outage will occur. Inherited from the superior OP of ODPSR, the throughput of this method is still better than SPSR-based schemes, as shown in Fig. 7. Moreover, the throughput of ODPSR and SPSR where ρ = 0.3 can converge to a saturation value when Ψ is large, e.g., $\Psi \geq 15$ dB. However, the throughput of SPSR where ρ = 0.7 is still much worse than others, even with a high source transmit power, i.e., Ψ = 15 dB. This means SPSR only attains the same throughput performance as ODPSR when the source transmit power is large and a suitable ρ value is applied. Otherwise, the throughput of SPSR is far inferior to that of ODPSR.

In Figs. 7 and 8, we investigate the effect of the power splitting ratio ρ on OP and throughput. The parameters are

This article has been accepted for publication in a future issue of this journal, but has not been fully edited. Content may change prior to final publication. Citation information: DOI 10.1109/JIOT.2021.3120766, IEEE Internet of Things Journal

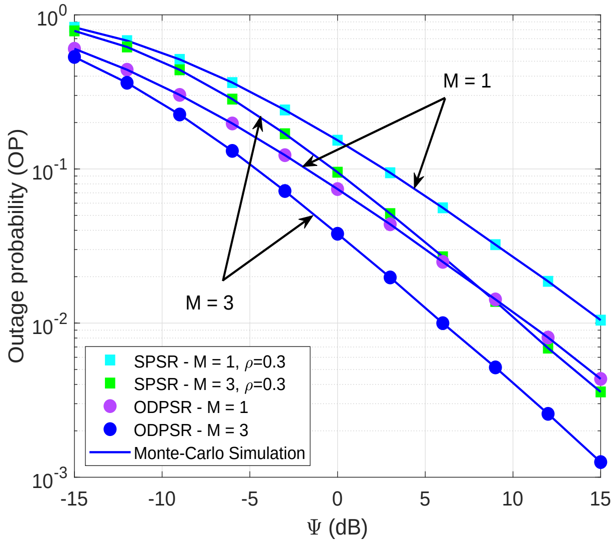

Fig. 3: OP versus Ψ with $\mathrm{C_{th}}$ = 1.25 (bps/Hz), η = 0.8, and Ω_a = 5, where $d_{\mathrm{SR}_m} = 0.3$ and d_{SR_m} = [0.3, 0.65, 0.8] corresponding to M = 1 and M = 3, respectively.

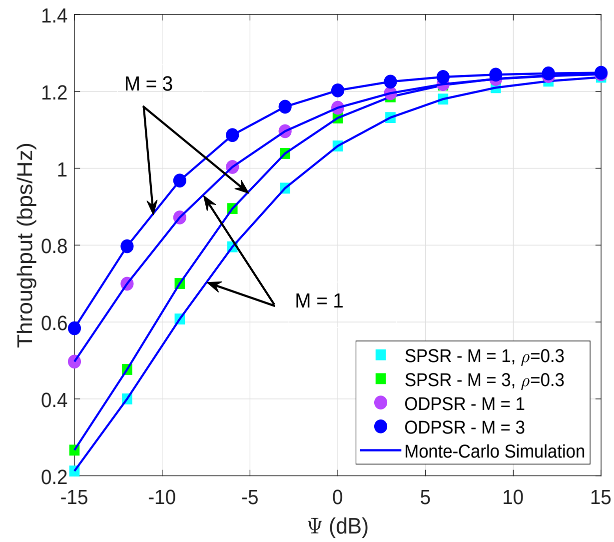

Fig. 4: Throughput versus Ψ with $\mathrm{C_{th}}$ = 1.25(bps/Hz), η = 0.8 and Ω_a = 5, where $d_{\mathrm{SR}_m} = 0.3$ and d_{SR_m} = [0.3, 0.65, 0.8] corresponding to M = 1 and M = 3, respectively.

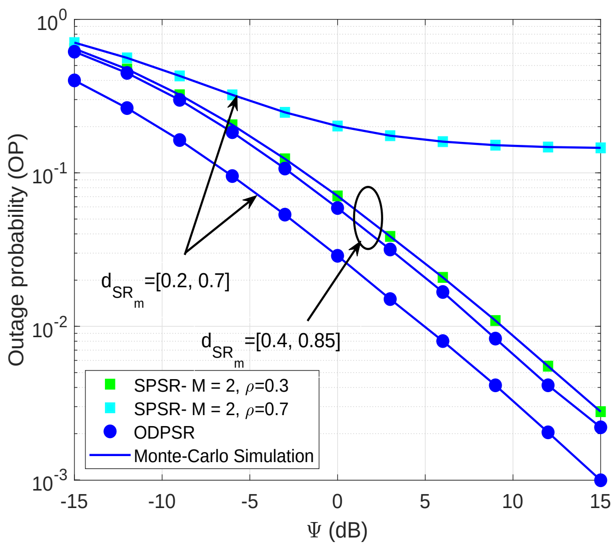

Fig. 5: OP versus Ψ with M = 2, $\mathrm{C_{th}}$ = 1.25 (bps/Hz), η = 0.8, and Ω_a = 5.

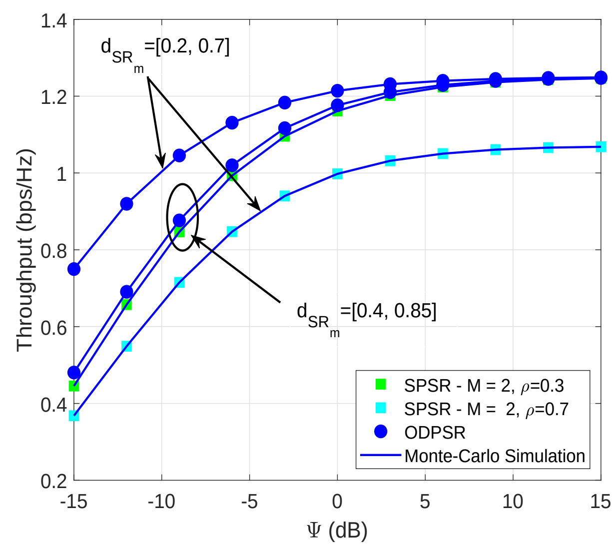

Fig. 6: Throughput versus Ψ with $\mathrm{C_{th}}$ = 1.25(bps/Hz), η = 0.8 and Ω_a = 5.

set at M = 2, $\mathrm{C_{th}}$ = 1.25 bps/Hz, η = 0.8, Ψ = 5 dB, and d_{SR} = [0.25, 0.65]. Notably, the power splitting ratio is a crucial factor because it not only affects the harvested energy at the relay but also the data transmission from relay R_m to destination D. Fig. 7 shows that for both SPSR-$\Omega_a = 0.5$ and SPSR-$\Omega_a = 2$, the outage decreased as ρ increased from 0 to the optimal ρ, but then decreased for a higher value of ρ. For instance, the optimal ρ equals 0.1 and 0.25, corresponding to SPSR-$\Omega_a = 0.5$ and SPSR-$\Omega_a = 2$, respectively. This is because a low amount of harvested energy is obtained with a small ρ, which results in a larger OP. However, when ρ is larger than the optimal value, more time is used for energy harvesting, while less time accounts for data transmission from $\mathrm{R}_m \rightarrow \mathrm{D}$, which also degrades the outage performance. This only exists for an optimal value of ρ maximizing the OP, which is obtained in ODPSR. This also explains why the outage performance of ODPSR for $\Omega_a = 0.5$ and ODPSR for $\Omega_a = 2$ is fixed with various ρ values. Fig. 8 plots the throughput of SPSR and ODPSR versus ρ. We can see that the throughput of ODPSR maintains a constant value with a varying value of ρ. In addition, ODPSR-based methods always outperform SPSR-based ones. This is expected since the inherent nature of ODPSR is to find the optimal power splitting ratio value which maximizes system capacity, as described in Section B.

This article has been accepted for publication in a future issue of this journal, but has not been fully edited. Content may change prior to final publication. Citation information: DOI 10.1109/JIOT.2021.3120766, IEEE Internet of Things Journal

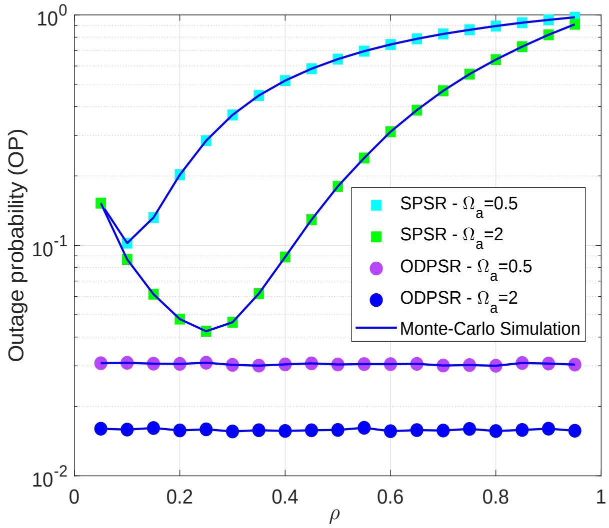

Fig. 7: OP versus ρ with M= 2, C_{th}=1.25 bps/Hz,η=0.8, Ψ = 5 dB, and d_{SR} = [0.25,0.65].

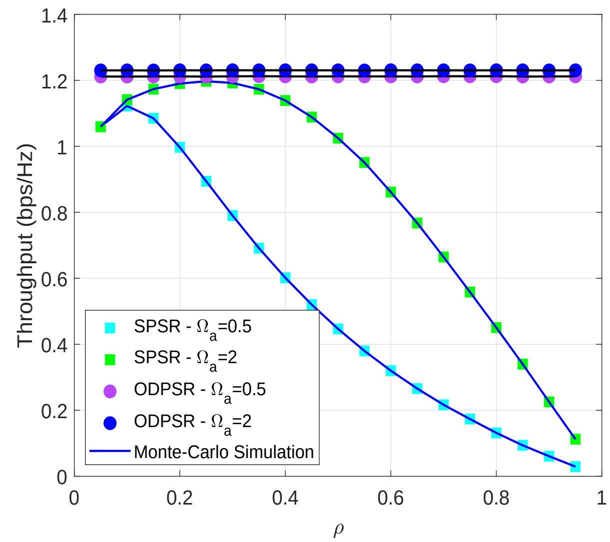

Fig. 8: Throughput versus ρ with M= 2, C_{th} = 1.25 (bps/Hz),η = 0.8, Ψ = 5 dB and d_{SR} = [0.25,0.65].

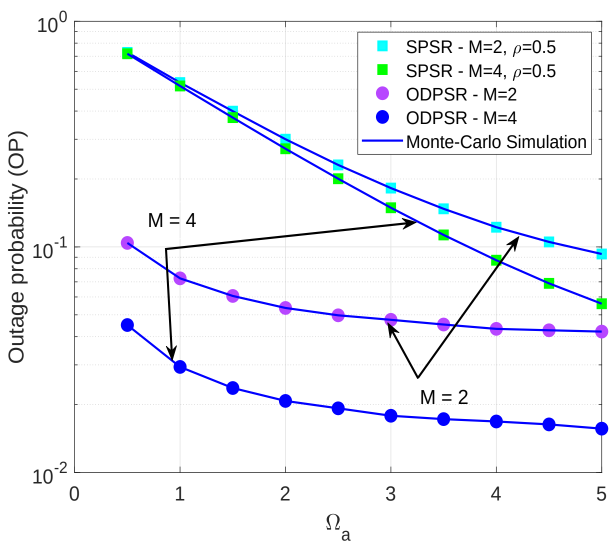

Fig. 9: OP versus Ω_a with η = 0.8, Ψ = 3 dB, C_{th} = 1.5 (bps/Hz), where d_{SR_m} = [0.35, 0.85] and d_{SR_m} = [0.25, 0.55, 0.4, 0.75] corresponding to M = 2 and M = 4, respectively.

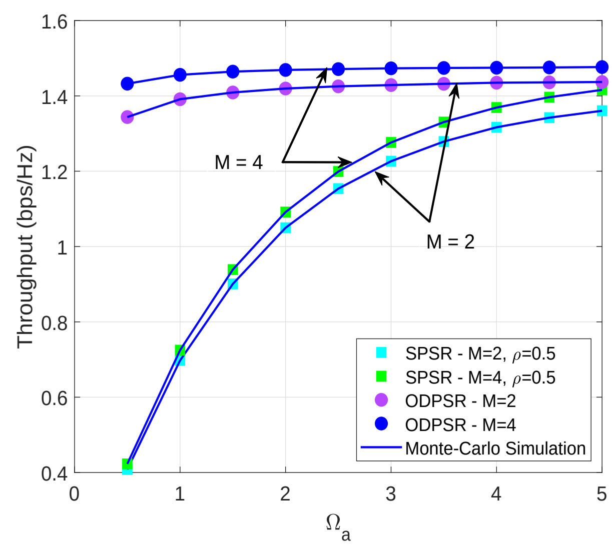

Fig. 10: Throughput vs. Ω_a with η = 0.8, Ψ = 3 dB, C_{th} = 1.5 (bps/Hz), where d_{SR_m} = [0.35, 0.85] and d_{SR_m} = [0.25, 0.55, 0.4, 0.75] corresponding to M = 2 and M = 4, respectively.

As the results show, the throughput of the SPSR-based scheme increased at the optimal ρ but then significantly decreased as ρ increased. This demonstrates the stability of ODPSR-based methods compared to SPSR-based methods.

Figs. 9 and 10 plot the effects of the residual self-interference parameter Ω_a at the relay in full-duplex operation on outage probability and throughput, where η = 0.8, Ψ = 3 dB and C_{th} = 1.5 bps/Hz. Fig. 9 indicates that ODPSR for M = 4 achieves the best results. Specifically, at Ω_a = 3, the OP values of ODPSR for M = 4, ODPSR for M = 2, SPSR for M = 4, SPSR for M = 2, were 0.0178, 0.0475, 0.1491, and 0.1823, respectively. Moreover, OP improved significantly as Ω_a increased. For example, at Ω_a = 0.5 and Ω_a = 2, the OP of ODPSR for M = 4 was 0.0451 and 0.0208, respectively. An explanation for this is that the higher the Ω_a, the lower the residual self-interference gain f_m at the relay, thereby reducing the effect of interference noise at the relay R_m and improving the system capacity. Fig. 10 shows the effect of Ω_a on throughput in each proposed method. We can observe that as Ω_a increased, the throughput of the SPSR-based methods dramatically improved. For example, at Ω_a = 2 and Ω_a = 4, the throughput of SPSR for M = 4 was 1.0916 and 1.3691 bps/Hz, respectively. However, the throughput performance of ODPSR-based methods only slightly improved as Ω_a increased.

This article has been accepted for publication in a future issue of this journal, but has not been fully edited. Content may change prior to final publication. Citation information: DOI 10.1109/JIOT.2021.3120766, IEEE Internet of Things Journal

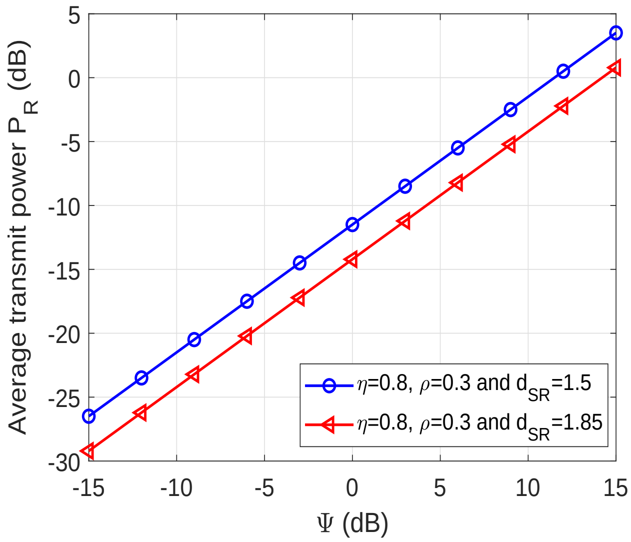

Fig. 11: P_{R} versus the transmit power-to-noise ratio Ψ.

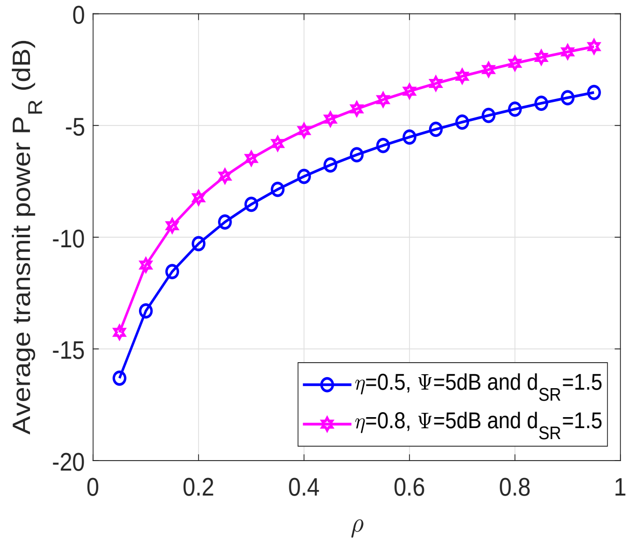

Fig. 12: P_{R} versus the power splitting ratio ρ.

This demonstrates that the residual self-interference has a more significant effect on SPSR than ODPSR. In other words, the ODPSR-based methods have better stability than SPSR-based methods. Figs. 4 to 10 clearly show that the analytical results closely match the simulation results for the proposed scheme, validating the analysis in Section IV.

Fig. 11 unveils the relationship between the transmit-power-to-noise Ψ and the average transmit power of the relay P_R. It is noted that since we assume that the transmission duration is normalized to 1, i.e., $T = 1$, the average transmit power, thus, can be considered as the average harvested energy too. It is no doubt that P_{R} increases linearly versus Ψ and confirms the accuracy of (10). Moreover, it is expected that the smaller the distance from S to R, the higher the harvested energy is achieved, improving the transmit power of the relay. Fig. 12 stretches the behavior of P_{R} regarding the PS ratio ρ. It is apparent that P_{R} is a monotonic increasing function of the ρ. Specifically, the larger the η is, the higher the P_{R} can be obtained.

V. Conclusion and Discussion

In the paper, we investigated the outage and throughput performance of a DF-based FD SWIPT relay network consisting of a source, multiple relays, and a destination under i.n.i.d. Rayleigh fading channels. By using the PS method and operating in FD mode, the relays could harvest energy from the source's signals. Closed-form expressions of the system OP and achievable throughput for SPSR and ODPSR schemes were derived. The theoretical analysis and numerical results indicated that the outage and throughput performance were highly dependent on the source's transmit power, the PS ratio, and the residual self-interference. It was observed that the performance of SPSR was shown to be far inferior to that of ODPSR. Nevertheless, when the source transmit power is high enough or when the self-interference has a small effect (i.e., $\Omega_a > 5$), the SPSR can obtain the same performance as ODPSR. Thus, the system is able to operate using SPSR with a simpler configuration. The outcome of this work will motivate a more general model that considers the Rician channel, which imposes new challenges and complexities but might enhance network performance.

Acknowledgment

This research was supported by the Ministry of Education, Youth and Sports of the Czech Republic under the grant SP2021/25 and e-INFRA CZ (ID:90140).

Appendix A: Proof of Theorem 1

First, the $\widetilde{\mathrm{OP}}$ in (24) can be calculated as

$$\begin{aligned}\widetilde{\mathrm{OP}} &= \sum_{a=1}^{M} \Pr\left(\gamma_{\mathrm{SR}_a} > Z_a, \varphi_a \le \frac{(1-\rho)}{\eta\rho\gamma_{\mathrm{th}}}, \Gamma_{\mathrm{R}_a\mathrm{D}} \ge \gamma_{\mathrm{th}}\right) \\ &= \sum_{a=1}^{M} \underbrace{\Pr\left(\varphi_a \le \frac{(1-\rho)}{\eta\rho\gamma_{\mathrm{th}}}\right)}_{\mathrm{P}_1} \underbrace{\Pr\left(\gamma_{\mathrm{SR}_a} > Z_a, \Gamma_{\mathrm{R}_a\mathrm{D}} \ge \gamma_{\mathrm{th}}\right)}_{\mathrm{P}_2}\end{aligned} \tag{41}$$

Based on (41), P_1 can be expressed as follows:

$$\mathrm{P}_1 = \Pr\left(\varphi_a \le \frac{(1-\rho)}{\eta\rho\gamma_{\mathrm{th}}}\right) = 1 - \exp\left[-\frac{\Omega_a(1-\rho)}{\eta\rho\gamma_{\mathrm{th}}}\right]. \tag{42}$$

This article has been accepted for publication in a future issue of this journal, but has not been fully edited. Content may change prior to final publication. Citation information: DOI 10.1109/JIOT.2021.3120766, IEEE Internet of Things Journal

Then, P_2 in (41) can be computed by

$$\begin{aligned} \mathrm{P}_2 &= \Pr\left(\gamma_{\mathrm{SR}_a} > Z_a, \eta\rho\Psi\gamma_{\mathrm{SR}_a}\gamma_{\mathrm{R}_a\mathrm{D}} \ge \gamma_{\mathrm{th}}\right) \\ &= \Pr\left(\gamma_{\mathrm{SR}_a} > Z_a\right) \\ &- \Pr\left(\gamma_{\mathrm{SR}_a} > Z_a, \eta\rho\Psi\gamma_{\mathrm{SR}_a}\gamma_{\mathrm{R}_a\mathrm{D}} < \gamma_{\mathrm{th}}\right) \\ &= \int_0^{+\infty} f_{Z_a}(z)\big(1 - F_{\gamma_{\mathrm{SR}_a}}(z)\big)dz \\ &- \int_0^{+\infty} f_{\lambda_{\mathrm{R}_a\mathrm{D}}}(y)\left[\int_0^{z_1}\int_z^{z_1} f_{Z_a}(z) f_{\lambda_{\mathrm{SR}_a}}(t)dzdt\right]dy \\ &= \int_0^{+\infty} \exp(-\lambda_{\mathrm{SR}_a}z) f_{Z_a}(z)dz \\ &- \int_0^{+\infty} f_{\lambda_{\mathrm{R}_a\mathrm{D}}}(y)\Big\{\int_0^{z_1} f_{Z_a}(z) f_{\lambda_{\mathrm{SR}_a}}(z, z_1)dz\Big\}dy, \quad (43) \end{aligned}$$

where

$$z_1 \triangleq \frac{\gamma_{\mathrm{th}}}{\eta\rho\Psi y}, \quad (44)$$

$$f_{\lambda_{\mathrm{SR}_a}}(z, z_1) \triangleq \left[\exp(-\lambda_{\mathrm{SR}_a}z) - \exp(-\lambda_{\mathrm{SR}_a}z_1)\right]. \quad (45)$$

Then, by substituting $f_{Z_a}(x)$ of Lemma 2 into (43), P_2 can be expressed as in (46), shown at the top of the next page.

Note that (46) still contains an integral. By adopting [45, Eq. (3.471.9)], the exact closed-form expression of P_2 is given as in (48), which is shown at the top of the next page.

By substituting (41), (42), (48) into (24), the $\mathrm{OP}_{\mathrm{SPSR}}$ can be obtained from (29), which completes the proof.

Appendix B: Proof of Lemma 1

Since we consider DF technique, the overall SNR of our system can be represented as in (16). The average throughput of the system is given as in (17). Therefore, to find the optimal value of the dynamic power splitting ratio $\rho^\star$, we need to solve the following optimization problem:

$$\mathcal{P}_1 : \max_{\rho} \quad (1 - \mathrm{OP}) \times \mathrm{C}_{\mathrm{DF}}, \quad (49)$$

$$\texttt{s.t.} \quad 0 \le \rho \le 1. \quad (50)$$

The problem $\mathcal{P}_1$ means we need to find the value of ρ to maximize the throughput $(1 - \mathrm{OP}) \times \mathrm{C}_{\mathrm{DF}}$ such that ρ ranges from 0 to 1. Because the OP and C_{DF} are expressed as $\mathrm{OP} = \Pr\left(\psi_{\mathrm{DF}} < \gamma_{th}\right)$ and $C_{\mathrm{DF}} = \log_2\left(1 + \psi_{\mathrm{DF}}\right)$, respectively, $\mathcal{P}_1$ is therefore equivalent to the following optimization problem:

$$\mathcal{P}_2 : \max_{\rho} \quad \Psi_{\mathrm{DF}} \quad (51)$$

$$\texttt{s.t.} \quad 0 \le \rho \le 1, \quad (52)$$

where $\Psi_{\mathrm{DF}} = \min\left(\Gamma_{\mathrm{SR}_m}, \Gamma_{\mathrm{R}_m\mathrm{D}}\right)$.

To clarify, Fig. 13 illustrates the Ψ_{DF} as a function of ρ. It shows that the values of Γ_{SR_m} linearly decrease and $\Gamma_{\mathrm{R}_m\mathrm{D}}$ linearly increase as ρ changes from 0 to 1. This can be explained based on the expressions of Γ_{SR_m} and $\Gamma_{\mathrm{R}_m\mathrm{D}}$ in (13) and (14). From Fig. 13, it is easy to see that the optimal value of $\rho^\star$ is obtained when $\Gamma_{\mathrm{SR}_m} = \Gamma_{\mathrm{R}_m\mathrm{D}}$, which completes the proof.

Appendix C: Proof of Lemma 3

From (31) and after some algebraic manipulations, $\rho^\star$ can be expressed as

$$\rho^\star = \frac{-\sqrt{4\eta^2\Psi\varphi_m\gamma_{\mathrm{SR}_m}\gamma_{\mathrm{R}_m\mathrm{D}} + 1} - 1}{2\eta^2\Psi\varphi_m\gamma_{\mathrm{SR}_m}\gamma_{\mathrm{R}_m\mathrm{D}}}, \quad (53)$$

or

$$\rho^* = \frac{\sqrt{4\eta^2\Psi\varphi_m\gamma_{\mathrm{SR}_m}\gamma_{\mathrm{R}_m\mathrm{D}} + 1} - 1}{2\eta^2\Psi\varphi_m\gamma_{\mathrm{SR}_m}\gamma_{\mathrm{R}_m\mathrm{D}}}. \quad (54)$$

Because $\rho^\star = \frac{-\sqrt{4\eta^2\Psi\varphi_m\gamma_{\mathrm{SR}_m}\gamma_{\mathrm{R}_m\mathrm{D}}+1}-1}{2\eta^2\Psi\varphi_m\gamma_{\mathrm{SR}_m}\gamma_{\mathrm{R}_m\mathrm{D}}} < 0$, $\rho^* = \frac{\sqrt{4\eta^2\Psi\varphi_m\gamma_{\mathrm{SR}_m}\gamma_{\mathrm{R}_m\mathrm{D}}+1}-1}{2\eta^2\Psi\varphi_m\gamma_{\mathrm{SR}_m}\gamma_{\mathrm{R}_m\mathrm{D}}}$ is selected as the optimal value of ρ. This completes the proof of Lemma 3.

Appendix D: Proof of Lemma 4

From (36), Θ can be re-written as

$$\begin{aligned} \Theta &= \int_0^{+\infty} f_{\gamma_{\mathrm{R}_a\mathrm{D}}}(y)\left[\int_0^{z_2}\int_z^{z_2} f_{Z_a}(z) f_{\gamma_{\mathrm{SR}_a}}(t)\, dzdt\right]dy \\ &= \int_0^{+\infty} f_{\gamma_{\mathrm{R}_a\mathrm{D}}}(y)\left[\int_0^{z_2} f_{Z_a}(z) f_{\lambda_{\mathrm{SR}_a}}(z, z_2)dz\right]dy, \quad (55) \end{aligned}$$

where

$$z_2 = \frac{\gamma_{th}(\eta\gamma_{th}x + 1)}{\eta\Psi y}, \quad (56)$$

$$f_{\lambda_{\mathrm{SR}_a}}(z, z_2) \triangleq \left[\exp(-\lambda_{\mathrm{SR}_a}z) - \exp(-\lambda_{\mathrm{SR}_a}z_2)\right]. \quad (57)$$

By applying Lemma 2, Θ can be expressed as in (58), which is shown at the top of the next page.

Then, by adopting [45, Eq. (3.324.1)], the exact closed-form expression of Θ is obtained as in (37). This completes the proof of Lemma 4.

Appendix E: Proof of Lemma 5

By substituting (37) into (35), we obtain

$$\begin{aligned} \Upsilon &= \sum_{u=1}^{M-1}(-1)^{u+1}\sum_{\substack{i_1=\cdots=i_u=1,\\ i_1<\cdots<i_u,\\ i_1,\ldots,i_u\neq a}}^{M}\lambda_1\frac{\lambda_{a,u}^{\mathrm{sum}}}{\lambda_{a,u}^{\mathrm{sum}} + \lambda_{\mathrm{SR}_a}} \\ &+ \sum_{u=1}^{M-1}(-1)^{u+1}\sum_{\substack{i_1=\cdots=i_u=1,\\ i_1<\cdots<i_u,\\ i_1,\ldots,i_u\neq a}}^{M}\int_0^{+\infty}\Omega_a\exp\left(-\Omega_a x\right)\Theta_1 dx. \end{aligned} \quad (59)$$

By denoting $y = \eta\gamma_{th}x + 1$, (59) can be expressed as

$$\begin{aligned} \Upsilon &= \sum_{u=1}^{M-1}(-1)^{u+1}\sum_{\substack{i_1=\cdots=i_u=1,\\ i_1<\cdots<i_u,\\ i_1,\ldots,i_u\neq a}}^{M}\lambda_1 + \sum_{u=1}^{M-1}(-1)^{u+1} \\ &\sum_{\substack{i_1=\cdots=i_u=1,\\ i_1<\cdots<i_u,\\ i_1,\ldots,i_u\neq a}}^{M}\frac{\Omega_a}{\eta\gamma_{th}}\exp\left(\frac{\Omega_a}{\eta\gamma_{th}}\right)\int_1^{+\infty}\exp\left(-\frac{\Omega_a y}{\eta\gamma_{th}}\right)\Theta_1 dy. \end{aligned} \quad (60)$$

This article has been accepted for publication in a future issue of this journal, but has not been fully edited. Content may change prior to final publication. Citation information: DOI 10.1109/JIOT.2021.3120766, IEEE Internet of Things Journal

$$
\begin{aligned}
\mathrm{P}_2 = & \sum_{u=1}^{M-1} (-1)^{u+1} \sum_{\substack{i_1=\cdots=i_u=1,\\ i_1<\cdots<i_u,\\ i_1,\ldots,i_u\neq a}}^{M} \int_0^{+\infty} \lambda_{a,u}^{\mathrm{sum}} \exp\left(-\lambda_{a,u}^{\mathrm{sum}} z - \lambda_{\mathrm{SR}_a} z\right) dz \\
& - \int_0^{+\infty} f_{\gamma_{\mathrm{R}_a\mathrm{D}}}(y) \left[\int_0^{z_1} \sum_{u=1}^{M-1} (-1)^{u+1} \sum_{\substack{i_1=\cdots=i_u=1,\\ i_1<\cdots<i_u,\\ i_1,\ldots,i_u\neq a}}^{M} \lambda_{a,u}^{\mathrm{sum}} \exp\left(-\lambda_{a,u}^{\mathrm{sum}} z\right) \times f_{\lambda_{\mathrm{SR}_a}}(z) dz \right] dy \\
= & \sum_{u=1}^{M-1} (-1)^{u+1} \sum_{\substack{i_1=\cdots=i_u=1,\\ i_1<\cdots<i_u,\\ i_1,\ldots,i_u\neq a}}^{M} \lambda_1 \\
& - \int_0^{+\infty} f_{\gamma_{\mathrm{R}_a\mathrm{D}}}(y) \left[\begin{array}{l} \displaystyle\sum_{u=1}^{M-1} (-1)^{u+1} \sum_{\substack{i_1=\cdots=i_u=1,\\ i_1<\cdots<i_u,\\ i_1,\ldots,i_u\neq a}}^{M} \lambda_1 \left[1 - \exp\left(-(\lambda_{a,u}^{\mathrm{sum}} + \lambda_{\mathrm{SR}_a}) z_1\right)\right] \\ \displaystyle -\sum_{u=1}^{M-1} (-1)^{u+1} \sum_{\substack{i_1=\cdots=i_u=1,\\ i_1<\cdots<i_u,\\ i_1,\ldots,i_u\neq a}}^{M} \exp\left(\lambda_{\mathrm{SR}_a} z_1\right) \left[1 - \exp\left(-\lambda_{a,u}^{\mathrm{sum}} z_1\right)\right] \end{array} \right] dy \\
= & \sum_{u=1}^{M-1} (-1)^{u+1} \sum_{\substack{i_1=\ldots=i_u=1,\\ i_1<\ldots<i_u,\\ i_1,\ldots,i_u\neq a}}^{M} \lambda_1 \\
& - \int_0^{+\infty} f_{\gamma_{\mathrm{R}_a\mathrm{D}}}(y) \sum_{u=1}^{M-1} (-1)^{u+1} \sum_{\substack{i_1=\cdots=i_u=1,\\ i_1<\cdots<i_u,\\ i_1,\ldots,i_u\neq a}}^{M} \left[\begin{array}{r} \lambda_1 - \exp\left(\lambda_{\mathrm{SR}_a} z_1\right) \\ \displaystyle + \frac{\lambda_{\mathrm{SR}_a}}{\lambda_{a,u}^{\mathrm{sum}} + \lambda_{\mathrm{SR}_a}} \exp\left(-(\lambda_{a,u}^{\mathrm{sum}} + \lambda_{\mathrm{SR}_a}) z_1\right) \end{array} \right] dy \\
= & \sum_{u=1}^{M-1} (-1)^{u+1} \sum_{\substack{i_1=\ldots=i_u=1,\\ i_1<\ldots<i_u,\\ i_1,\ldots,i_u\neq a}}^{M} \int_0^{+\infty} \lambda_{\mathrm{R}_a\mathrm{D}} \times \exp\left(-\lambda_{\mathrm{R}_a\mathrm{D}} y - \lambda_{\mathrm{SR}_a} z_1\right) dy \\
& - \sum_{u=1}^{M-1} (-1)^{u+1} \sum_{\substack{i_1=\cdots=i_u=1,\\ i_1<\cdots<i_u,\\ i_1,\ldots,i_u\neq a}}^{M} \lambda_1 \int_0^{+\infty} \lambda_{\mathrm{R}_a\mathrm{D}} \times \exp\left(-\lambda_{\mathrm{R}_a\mathrm{D}} y - (\lambda_{a,u}^{\mathrm{sum}} + \lambda_{\mathrm{SR}_a}) z_1\right) dy,
\end{aligned} \tag{46}
$$

where $\lambda_1 \triangleq \dfrac{\lambda_{a,u}^{\mathrm{sum}}}{\lambda_{a,u}^{\mathrm{sum}} + \lambda_{\mathrm{SR}_a}}$. (47)

$$
\mathrm{P}_2 = -\sum_{u=1}^{M-1} (-1)^{u+1} \sum_{\substack{i_1=\cdots=i_u=1,\\ i_1<\cdots<i_u,\\ i_1,\ldots,i_u\neq a}}^{M} \left[\begin{array}{r} \displaystyle \frac{2\lambda_{\mathrm{SR}_a}}{\lambda_{a,u}^{\mathrm{sum}} + \lambda_{\mathrm{SR}_a}} \times \sqrt{\frac{\left(\lambda_{a,u}^{\mathrm{sum}} + \lambda_{\mathrm{SR}_a}\right) \lambda_{\mathrm{R}_a\mathrm{D}} \gamma_{\mathrm{th}}}{\eta\rho\Psi}} \times K_1\left(2\sqrt{\frac{\left(\lambda_{a,u}^{\mathrm{sum}} + \lambda_{\mathrm{SR}_a}\right) \lambda_{\mathrm{R}_a\mathrm{D}} \gamma_{\mathrm{th}}}{\eta\rho\Psi}}\right) \\ \displaystyle -2\sqrt{\frac{\lambda_{\mathrm{SR}_a} \lambda_{\mathrm{R}_a\mathrm{D}} \gamma_{\mathrm{th}}}{\eta\rho\Psi}} \times K_1\left(2\sqrt{\frac{\lambda_{\mathrm{SR}_a} \lambda_{\mathrm{R}_a\mathrm{D}} \gamma_{\mathrm{th}}}{\eta\rho\Psi}}\right) \end{array} \right]. \tag{48}
$$

This article has been accepted for publication in a future issue of this journal, but has not been fully edited. Content may change prior to final publication. Citation information: DOI 10.1109/JIOT.2021.3120766, IEEE Internet of Things Journal

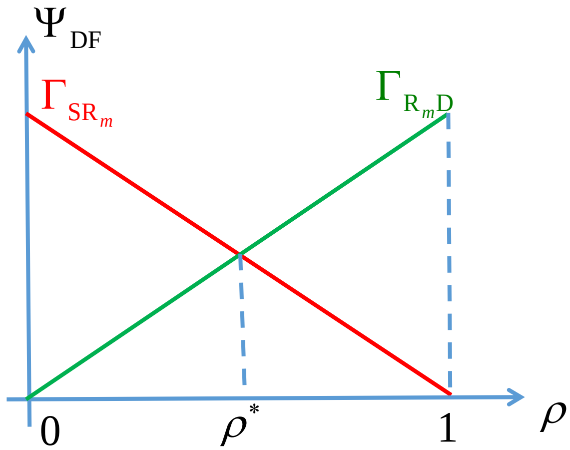

Fig. 13: Illustration of the Γ_{SR_m} and $\Gamma_{\mathrm{R}_m\mathrm{D}}$ as a function of ρ.

To simplify analysis, we adopt the Taylor Series, as follows:

$$\exp\left(-\frac{\Omega_a y}{\eta\gamma_{th}}\right) = \sum_{t=0}^{\infty} \frac{\left(-\frac{\Omega_a y}{\eta\gamma_{th}}\right)^t}{t!} = \sum_{t=0}^{\infty} (-1)^t \frac{\left(\frac{\Omega_a}{\eta\gamma_{th}}\right)^t}{t!} y^t. \tag{61}$$

By substituting (61) into (60), we have

$$\begin{aligned}\Upsilon = &\sum_{u=1}^{M-1} (-1)^{u+1} \sum_{\substack{i_1=\cdots=i_u=1,\\ i_1<\cdots<i_u,\\ i_1,\ldots,i_u\neq a}}^{M} \frac{\lambda_{a,u}^{\mathrm{sum}}}{\lambda_{a,u}^{\mathrm{sum}} + \lambda_{\mathrm{SR}_a}} \\ &+ \sum_{u=1}^{M-1} (-1)^{u+1} \sum_{\substack{i_1=\cdots=i_u=1,\\ i_1<\cdots<i_u,\\ i_1,\ldots,i_u\neq a}}^{M} \left[\begin{array}{c} \frac{\Omega_a}{\eta\gamma_{th}} \exp\left(\frac{\Omega_a}{\eta\gamma_{th}}\right) \\ \times \int_1^{+\infty} \sum_{t=0}^{\infty} (-1)^t \frac{\left(\frac{\Omega_a}{\eta\gamma_{th}}\right)^t}{t!} \end{array}\right] \\ &\times \left[\begin{array}{r} \frac{2\lambda_{\mathrm{SR}_a}\vartheta}{\lambda_{a,u}^{\mathrm{sum}} + \lambda_{\mathrm{SR}_a}} \times y^{t+0.5} \times K_1\left(2\vartheta\sqrt{y}\right) \\ -2\zeta y^{t+0.5} \times K_1\left(2\zeta\sqrt{y}\right) \end{array}\right] dy, \end{aligned} \tag{62}$$

where

$$\vartheta = \sqrt{\frac{\left(\lambda_{a,u}^{\mathrm{sum}} + \lambda_{\mathrm{SR}_a}\right)\lambda_{\mathrm{R}_a\mathrm{D}}\gamma_{\mathrm{th}}}{\eta\Psi}}, \tag{63}$$

$$\zeta = \sqrt{\frac{\lambda_{\mathrm{SR}_a}\lambda_{\mathrm{R}_a\mathrm{D}}\gamma_{\mathrm{th}}}{\eta\Psi}}. \tag{64}$$

By adopting [45, Eq. (6.592.4)], the exact closed-form expression of Υ can be obtained as in Lemma 5. This completes the proof.

References

[1] Ericsson, "Ericsson mobility report: November 2019," 2019.
[2] P. X. Nguyen, D. H. Tran, O. Onireti, P. T. Tin, S. Q. Nguyen, S. Chatzinotas, and H. V. Poor, "Backscatter-Assisted Data Offloading in OFDMA-based Wireless Powered Mobile Edge Computing for IoT Networks," *IEEE Internet Things J.*, pp. 1–1, 2021.
[3] T. V. Nguyen, T. N. Tran, K. Shim, T. Huynh-The, and B. An, "A Deep Neural Network-based Relay Selection Scheme in Wireless-Powered Cognitive IoT Networks," *IEEE Internet Things J.*, pp. 1–1, 2020.
[4] B. Mao, Y. Kawamoto, and N. Kato, "AI-Based Joint Optimization of QoS and Security for 6G Energy Harvesting Internet of Things," *IEEE Internet of Things J.*, vol. 7, no. 8, pp. 7032–7042, 2020.
[5] T. D. Hieu, L. T. Dung, and B.-S. Kim, "Stability-aware geographic routing in energy harvesting wireless sensor networks," *Sensors*, vol. 16, no. 5, p. 696, 2016.
[6] X. Lu, P. Wang, D. Niyato, D. I. Kim, and Z. Han, "Wireless Networks With RF Energy Harvesting: A Contemporary Survey," *IEEE Commun. Surv. Tutor.*, vol. 17, no. 2, pp. 757–789, 2015.
[7] T. N. Nguyen, T. H. Q. Minh, P. T. Tran, M. Voznak, T. T. Duy, T.-L. Nguyen, and P. T. Tin, "Performance enhancement for energy harvesting based two-way relay protocols in wireless ad-hoc networks with partial and full relay selection methods," *Ad hoc Networks*, vol. 84, pp. 178–187, 2019.
[8] K. W. Choi, A. A. Aziz, D. Setiawan, N. M. Tran, L. Ginting, and D. I. Kim, "Distributed Wireless Power Transfer System for Internet of Things Devices," *IEEE Internet Things J.*, vol. 5, no. 4, pp. 2657–2671, 2018.
[9] T. D. Hieu, T. T. Duy, and B. Kim, "Performance Enhancement for Multihop Harvest-to-Transmit WSNs With Path-Selection Methods in Presence of Eavesdroppers and Hardware Noises," *IEEE Sens. J.*, vol. 18, no. 12, pp. 5173–5186, 2018.
[10] Q. Wu, G. Zhang, D. W. K. Ng, W. Chen, and R. Schober, "Generalized Wireless-Powered Communications: When to Activate Wireless Power Transfer?" *IEEE Trans. Veh. Technol.*, vol. 68, no. 8, pp. 8243–8248, 2019.
[11] P. T. Tin, B. H. Dinh, T. N. Nguyen, D. H. Ha, and T. T. Trang, "Power Beacon-Assisted Energy Harvesting Wireless Physical Layer Cooperative Relaying Networks: Performance Analysis," *Symmetry*, vol. 12, no. 1, p. 106, 2020.
[12] L. R. Varshney, "Transporting information and energy simultaneously," in *Proc. IEEE Int. Symp. Inf. Theory, Toronto, ON, Canada*, 2008, pp. 1612–1616.
[13] P. Grover and A. Sahai, "Shannon meets Tesla: Wireless information and power transfer," in *Proc. IEEE Int. Symp. Inf. Theory*, 2010, pp. 2363–2367.
[14] R. Zhang and C. K. Ho, "MIMO Broadcasting for Simultaneous Wireless Information and Power Transfer," *IEEE Trans. Wireless Commun.*, vol. 12, no. 5, pp. 1989–2001, 2013.
[15] I. Krikidis, S. Timotheou, S. Nikolaou, G. Zheng, D. W. K. Ng, and R. Schober, "Simultaneous wireless information and power transfer in modern communication systems," *IEEE Commun. Mag.*, vol. 52, no. 11, pp. 104–110, 2014.
[16] A. A. Nasir, X. Zhou, S. Durrani, and R. A. Kennedy, "Wireless-Powered Relays in Cooperative Communications: Time-Switching Relaying Protocols and Throughput Analysis," *IEEE Trans. Commun.*, vol. 63, no. 5, pp. 1607–1622, 2015.
[17] H. Ding, X. Wang, D. B. da Costa, Y. Chen, and F. Gong, "Adaptive Time-Switching Based Energy Harvesting Relaying Protocols," *IEEE Trans. Commun.*, vol. 65, no. 7, pp. 2821–2837, 2017.
[18] H. Tran-Dinh, S. Chatzinotas, and B. Ottersten, "Throughput Maximization for Wireless Communication Systems with Backscatter- and Cache-assisted UAV Technology," *in Arxiv*, preprint arXiv:2011.07955.
[19] J. Wang, G. Wang, B. Li, H. Yang, Y. Hu, and A. Schmeink, "Massive MIMO Two-Way Relaying Systems with SWIPT in IoT Networks," *IEEE Internet Things J.*, pp. 1–1, 2020.
[20] T. N. Nguyen, M. Tran, T.-L. Nguyen, D.-H. Ha, and M. Voznak, "Performance Analysis of a User Selection Protocol in Cooperative Networks with Power Splitting Protocol-Based Energy Harvesting over Nakagami-m/Rayleigh Channels," *Electronics*, vol. 8, no. 4, p. 448, 2019.
[21] Y. Zou, J. Zhu, and X. Jiang, "Joint Power Splitting and Relay Selection in Energy-Harvesting Communications for IoT Networks," *IEEE Internet Things J.*, vol. 7, no. 1, pp. 584–597, 2020.
[22] A. Alsharoa, H. Ghazzai, A. E. Kamal, and A. Kadri, "Optimization of a power splitting protocol for two-way multiple energy harvesting relay system," *IEEE Trans. Green Commun. Netw.*, vol. 1, no. 4, pp. 444–457, 2017.
[23] D. H. Ha, T. N. Nguyen, M. H. Q. Tran, X. Li, P. T. Tran, and M. Voznak, "Security and Reliability Analysis of a Two-Way Half-Duplex Wireless Relaying Network Using Partial Relay Selection and Hybrid TPSR Energy Harvesting at Relay Nodes," *IEEE Access*, vol. 8, pp. 187 165–187 181, 2020.
[24] T. N. Nguyen, P. T. Tran, and M. Voznak, "Wireless Energy Harvesting Meets Receiver diversity: A Successful Approach for Two-Way Half-Duplex Relay Networks over Block Rayleigh Fading Channel," *Computer Networks*, vol. 172, p. 107176, 2020.

$$
\begin{aligned}
\Theta &= \int_0^{+\infty} f_{\gamma_{\mathrm{R}_a\mathrm{D}}}(y) \left[\int_0^{z_2} \left\{ \begin{array}{c} \sum\limits_{u=1}^{M-1} (-1)^{u+1} \sum\limits_{\substack{i_1=\ldots=i_u=1,\\ i_1<\ldots<i_u,\\ i_1,\ldots,i_u\neq a}}^{M} \lambda_{a,u}^{\mathrm{sum}} \exp\left(-\lambda_{a,u}^{\mathrm{sum}} z\right) \times \\ \left(\exp\left(-\lambda_{\mathrm{SR}_a} z\right) - \exp\left(-\lambda_{\mathrm{SR}_a} z_2\right)\right) \end{array} \right\} dz \right] dy \\
&= \int_0^{+\infty} f_{\gamma_{\mathrm{R}_a\mathrm{D}}}(y) \left[\begin{array}{c} \sum\limits_{u=1}^{M-1} (-1)^{u+1} \sum\limits_{\substack{i_1=\cdots=i_u=1,\\ i_1<\cdots<i_u,\\ i_1,\ldots,i_u\neq a}}^{M} \lambda_1 \left[1 - \exp\left(-\left(\lambda_{a,u}^{\mathrm{sum}} + \lambda_{\mathrm{SR}_a}\right) z_2\right)\right] \\ - \sum\limits_{u=1}^{M-1} (-1)^{u+1} \sum\limits_{\substack{i_1=\cdots=i_u=1,\\ i_1<\cdots<i_u,\\ i_1,\ldots,i_u\neq a}}^{M} \exp\left(-\lambda_{\mathrm{SR}_a} z_2\right) \left[1 - \exp\left(-\lambda_{a,u}^{\mathrm{sum}} z_2\right)\right] \end{array} \right] dy \\
&= \int_0^{+\infty} f_{\gamma_{\mathrm{R}_a\mathrm{D}}}(y) \sum_{u=1}^{M-1} (-1)^{u+1} \sum_{\substack{i_1=\ldots=i_u=1,\\ i_1<\cdots<i_u,\\ i_1,\ldots,i_u\neq a}}^{M} \left[\begin{array}{r} \lambda_1 - \exp\left(-\lambda_{\mathrm{SR}_a} z_2\right) \\ + \dfrac{\lambda_{\mathrm{SR}_a}}{\lambda_{a,u}^{\mathrm{sum}} + \lambda_{\mathrm{SR}_a}} \exp\left(-\left(\lambda_{a,u}^{\mathrm{sum}} + \lambda_{\mathrm{SR}_a}\right) z_2\right) \end{array} \right] dy \\
&= \sum_{u=1}^{M-1} (-1)^{u+1} \sum_{\substack{i_1=\cdots=i_u=1,\\ i_1<\cdots<i_u,\\ i_1,\ldots,i_u\neq a}}^{M} \lambda_1 - \sum_{u=1}^{M-1} (-1)^{u+1} \sum_{\substack{i_1=\cdots=i_u=1,\\ i_1<\cdots<i_u,\\ i_1,\ldots,i_u\neq a}}^{M} \int_0^{+\infty} \lambda_{\mathrm{R}_a\mathrm{D}} \times \exp\left(-\lambda_{\mathrm{R}_a\mathrm{D}} y - \lambda_{\mathrm{SR}_a} z_2\right) dy \\
&+ \sum_{u=1}^{M-1} (-1)^{u+1} \sum_{\substack{i_1=\cdots=i_u=1,\\ i_1<\cdots<i_u,\\ i_1,\ldots,i_u\neq a}}^{M} \frac{\lambda_{\mathrm{SR}_a}}{\lambda_{a,u}^{\mathrm{sum}} + \lambda_{\mathrm{SR}_a}} \int_0^{+\infty} \lambda_{\mathrm{R}_a\mathrm{D}} \times \exp\left(-\lambda_{\mathrm{R}_a\mathrm{D}} y - \left(\lambda_{a,u}^{\mathrm{sum}} + \lambda_{\mathrm{SR}_a}\right) z_2\right) dy. \qquad (58)
\end{aligned}
$$

[25] X. Liu and X. Zhang, "Rate and Energy Efficiency Improvements for 5G-Based IoT With Simultaneous Transfer," *IEEE Internet of Things J.*, vol. 6, no. 4, pp. 5971–5980, 2019.

[26] E. Boshkovska, D. W. K. Ng, N. Zlatanov, and R. Schober, "Practical Non-Linear Energy Harvesting Model and Resource Allocation for SWIPT Systems," *IEEE Commun. Lett.*, vol. 19, no. 12, pp. 2082–2085, 2015.

[27] A. Sabharwal, P. Schniter, D. Guo, D. W. Bliss, S. Rangarajan, and R. Wichman, "In-Band Full-Duplex Wireless: Challenges and Opportunities," *IEEE J. Sel. Areas Commun.*, vol. 32, no. 9, pp. 1637–1652, 2014.

[28] D. Bharadia, E. McMilin, and S. Katti, "Full duplex radios," in *Proc. ACM SIGCOMM 2013*, 2013, pp. 375–386.

[29] D. H. Tran, V. D. Nguyen, S. Gautam, S. Chatzinotas, T. X. Vu, and B. Ottersten, "Resource Allocation for UAV Relay-Assisted IoT Communication Networks," in *Proc. 2020 IEEE Globecom Workshops (GC Wkshps)*, 2020, pp. 1–7.

[30] Z. Zhang, K. Long, A. V. Vasilakos, and L. Hanzo, "Full-Duplex Wireless Communications: Challenges, Solutions, and Future Research Directions," *Proc. IEEE*, vol. 104, no. 7, pp. 1369–1409, 2016.

[31] T. Zhang, C. Su, A. Najafi, and J. C. Rudell, "Wideband Dual-Injection Path Self-Interference Cancellation Architecture for Full-Duplex Transceivers," *IEEE J. Solid-State Circuits*, vol. 53, no. 6, pp. 1563–1576, 2018.

[32] H. Huang, S. Hu, T. Yang, and C. W. Yuan, "Full Duplex Non-orthogonal Multiple Access with Layers-based Optimized Mobile Relays Subsets Algorithm in B5G/6G Ubiquitous Networks," *IEEE Internet of Things J.*, pp. 1–1, 2020.

[33] R. Askar, J. Chung, Z. Guo, H. Ko, W. Keusgen, and T. Haustein, "Interference Handling Challenges toward Full Duplex Evolution in 5G and Beyond Cellular Networks," *IEEE Wireless Commun.*, vol. 28, no. 1, pp. 51–59, 2021.

[34] T. N. Nguyen, M. Tran, T. L. Nguyen, and M. Voznak, "Adaptive relaying protocol for decode and forward full-duplex system over Rician fading channel: System performance analysis," *China Commun.*, vol. 16, no. 3, pp. 92–102, 2019.

[35] D. Xu and H. Zhu, "Secure Transmission for SWIPT IoT Systems With Full-Duplex IoT Devices," *IEEE Internet Things J.*, vol. 6, no. 6, pp. 10 915–10 933, 2019.

[36] Y. Dong, A. El Shafie, M. J. Hossain, J. Cheng, N. Al-Dhahir, and V. C. M. Leung, "Secure Beamforming in Full-Duplex MISO-SWIPT Systems With Multiple Eavesdroppers," *IEEE Trans. Wireless Commun.*, vol. 17, no. 10, pp. 6559–6574, 2018.

[37] K. G. Wu, F. T. Chien, Y. F. Lin, and M. K. Chang, "SINR and Delay Analyses in Two-Way Full-Duplex SWIPT-Enabled Relaying Systems," *IEEE Trans. Commun.*, pp. 1–1, 2020.

[38] Y. Zeng and R. Zhang, "Full-duplex wireless-powered relay with self-energy recycling," *IEEE Wireless Communications Letters*, vol. 4, no. 2, pp. 201–204, 2015.

[39] M. Zhao, Q. Shi, Y. Cai, and M. Zhao, "Joint transceiver design for full-duplex cloud radio access networks with swipt," *IEEE Transactions on Wireless Communications*, vol. 16, no. 9, pp. 5644–5658, 2017.

[40] A. Goldsmith, *Wireless communications*. Cambridge university press, 2005.

[41] N. T. Do, V. N. Q. Bao, and B. An, "Outage Performance Analysis of Relay Selection Schemes in Wireless Energy Harvesting Cooperative Networks over Non-Identical Rayleigh Fading Channels," *Sensors*, vol. 16, no. 3, p. 295, 2016.

[42] L. T. Dung, T. D. Hieu, S.-G. Choi, B.-S. Kim, B. An *et al.*, "Impact of beamforming on the path connectivity in cognitive radio ad hoc networks," *Sensors*, vol. 17, no. 4, p. 690, 2017.

[43] H. Tran-Dinh, T. X. Vu, S. Chatzinotas, and B. Ottersten, "Energy-efficient Trajectory Design for UAV-enabled Wireless Communications with Latency Constraints," in *2019 53rd Asilomar Conference on Signals, Systems, and Computers*, 2019, pp. 347–352.

[44] L. T. Dung, T. D. Hieu, B. An, B.-S. Kim *et al.*, "How does beamforming influence the connectivity of cognitive radio ad-hoc networks?" in *2016 International Symposium on Computer, Consumer and Control (IS3C)*. IEEE, 2016, pp. 227–230.

[45] A. Jeffrey and D. Zwillinger, *Table of Integrals, Series, and Products - Seventh Edition*. Elsevier, 2007.

Tan N. Nguyen (nguyennhattan@tdtu.edu.vn) was born in 1986 in Nha Trang City, Vietnam. He received a BS degree in electronics in 2008 from Ho Chi Minh University of Natural Sciences and an MS degree in telecommunications engineering in 2012 from Vietnam National University. He received a PhD in communications technologies in 2019 from the Faculty of Electrical Engineering and Computer Science at VSB Technical University of Ostrava, Czech Republic. He joined the Faculty of Electrical and Electronics Engineering of Ton Duc Thang University, Vietnam, in 2013, and since then as been lecturing. His major interests are cooperative communications, cognitive radio, and physical layer security.

Dinh-Hieu Tran (S'20) was born and grew up in Gia Lai, Vietnam (1989). He received the B.E. degree in Electronics and Telecommunication Engineering Department from Ho Chi Minh City University of Technology, Vietnam, in 2012. In 2017, he finished the M.Sc degree in Electronics and Computer Engineering from Hongik University (Hons.), South Korea. He is currently pursuing the Ph.D. degree at the Interdisciplinary Centre for Security, Reliability and Trust (SnT), University of Luxembourg, under the supervision of Prof. Symeon Chatzinotas and Prof. Björn Ottersten. His research interests include UAVs, IoTs, Mobile Edge Computing, Caching, Backscatter, B5G for wireless communication networks. He was a co-recipient of the IS3C 2016 best paper award.

Van-Duc Phan (duc.pv@vlu.edu.vn) was born in 1975 in Long An province, Vietnam. He received his MS degree from the Department of Electric, Electrical and Telecommunications Engineering at Ho Chi Minh City University of Transport in Vietnam and then in 201 a PhD from the Department of Mechanical and Automation Engineering, Da-Yeh University, Taiwan. His current research interests are sliding mode controls, non-linear systems and active magnetic bearings, flywheel energy storage systems, power system optimization, optimization algorithms, renewable energies, energy harvesting (EH) enabled cooperative networks, optical property improvement, lighting performance of white LEDs, energy efficiency LED driver integrated circuits, novel radio access technologies, and physical security in communications networks.

Miroslav Voznak (M'09-SM'16) received his PhD in telecommunications in 2002 from the Faculty of Electrical Engineering and Computer Science at VSB Technical University of Ostrava, and achieved habilitation in 2009. He was appointed Full Professor in Electronics and Communications Technologies in 2017. His research interests generally focus on ICT, especially quality of service and experience, network security, wireless networks, and big data analytics. He has authored and co-authored over one hundred articles indexed in SCI/SCIE journals. According to the Stanford University study released in 2020, he is one of the Worlds Top 2% of scientists in Networking & Telecommunications and Information & Communications Technologies. He served as a general chair of the 11^{th} IFIP Wireless and Mobile Networking Conference in 2018 and the 24^{th} IEEE/ACM International Symposium on Distributed Simulation and Real Time Applications in 2020. He participated in six projects funded by EU in programs managed directly by European Commission. Currently, he is a principal investigator in the research project QUANTUM5 funded by NATO, which focuses on the application of quantum cryptography in 5G campus networks.

Symeon Chatzinotas , (S'06-M'09-SM'13) is currently Full Professor / Chief Scientist I in Satellite Communications and Head of the SIGCOM Research Group at SnT, University of Luxembourg. He coordinates research activities in communications and networking, acting as a PI in over 20 projects and is the main representative for 3GPP, ETSI, DVB. In the past, he worked as a Visiting Professor at the University of Parma, Italy, lecturing on 5G Wireless Networks. He was involved in numerous R&D projects for NCSR Demokritos, CERTH Hellas and CCSR, University of Surrey. He was co-recipient of the 2014 IEEE Distinguished Contributions to Satellite Communications Award and Best Paper Awards at EURASIP JWCN, CROWNCOM, ICSSC. He has (co-)authored more than 450 technical papers in refereed international journals, conferences and scientific books. He is currently on the editorial board of the IEEE Transactions on Communications, IEEE Open Journal of Vehicular Technology, and the International Journal of Satellite Communications and Networking.

Björn Ottersten , (S'87-M'89-SM'99-F'04) was born in Stockholm, Sweden, in 1961. He received his MS degree in electrical engineering and applied physics from Linkping University, Linkping, Sweden, in 1986, and a PhD degree in electrical engineering from Stanford University, Stanford, CA, USA, in 1990. He has held research positions with the Department of Electrical Engineering at Linkping University, the Information Systems Laboratory at Stanford University, the Katholieke Universiteit Leuven in Belgium, and the University of Luxembourg. From 1996 to 1997, he was the Director of Research at ArrayComm, Inc., a start-up in San Jose, CA, USA, based on his patented technology. In 1991, he was appointed professor of signal processing at the Royal Institute of Technology (KTH) in Stockholm, Sweden. Dr. Ottersten has been Head of the Department for Signals, Sensors, and Systems, KTH, and Dean of the School of Electrical Engineering, KTH. He is currently the Director for the Interdisciplinary Centre for Security, Reliability and Trust at the University of Luxembourg. He is a recipient of the IEEE Signal Processing Society Technical Achievement Award and been twice awarded the European Research Council advanced research grant. He has co-authored journal papers which received the IEEE Signal Processing Society Best Paper Award in 1993, 2001, 2006, 2013, and 2019, and eight IEEE conference papers best paper awards. He has been a board member of IEEE Signal Processing Society and the Swedish Research Council and currently serves on the boards of EURASIP and the Swedish Foundation for Strategic Research. He has served as an Associate Editor for the IEEE TRANSACTIONS ON SIGNAL PROCESSING and the Editorial Board of the IEEE Signal Processing Magazine. He is currently a member of the editorial boards of the IEEE Open Journal of Signal Processing, EURASIP Signal Processing Journal, EURASIP Journal of Advanced Signal Processing and Foundations and Trends of Signal Processing. He is a fellow of EURASIP.

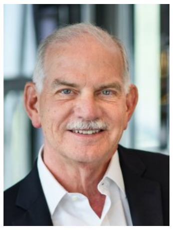

H. Vincent Poor (S72, M77, SM82, F87) received his PhD in EECS from Princeton University in 1977. From 1977 to 1990, he was at the faculty of the University of Illinois at Urbana-Champaign. Since 1990, he has been on the faculty at Princeton, where he is the Michael Henry Strater University Professor. From 2006 to 2016, he also served as the Dean of Princetons School of Engineering and Applied Science. Dr. Poors research interests are in the areas of information theory, machine learning and network science and their application in wireless networks, energy systems, and related fields. Among his publications in these areas is the forthcoming book "*Machine Learning and Wireless Communications*" (Cambridge University Press, 2021). Dr. Poor is a member of the National Academy of Engineering and the National Academy of Sciences. He is a foreign member of the Chinese Academy of Sciences, the Royal Society, and other national and international academies. Recent recognition of his work includes the 2017 IEEE Alexander Graham Bell Medal and a D.Eng. *honoris causa* from the University of Waterloo, awarded in 2019.